8-1-2009

Gas-phase surface oxidation and chlorination of carbon nanotubes

Luciana C. Oliveira

Gas-phase Surface Oxidation and Chlorination of Carbon Nanotubes

Luciana C. Oliveira

August 2009

Thesis Submitted in Partial Fulfillment of the Requirements for the Degree of

Master of Science in Chemistry

Approved:

_____

Research Advisor
Dr. Gerald A. Takacs

_____

Department Head
Dr. L. Paul Rosenberg

Department of Chemistry

Rochester Institute of Technology

Rochester, New York 14623

Copyright Release Form

Gas-phase Surface Oxidation and Chlorination of Carbon Nanotubes

I, Luciana C. Oliveira, hereby grant permission to the Wallace Memorial Library of the Rochester Institute of Technology to reproduce this thesis in its entirety or in part. Any reproduction will be with the intent to contribute to the proliferation of knowledge and understanding in the scientific community and will not be for commercial use or profit.

_____ _____

Luciana C. Oliveira Date

Table of Contents

Acknowledgements

I would like to primarily thank my advisor, Dr. G. A. Takacs for his guidance, patience, support and encouragement throughout the development of my research project in the M. S. program at RIT. I am also thankful for the time and assistance provided by my research committee, Dr. L. P. Rosenberg, Dr. A. Entenberg and Dr. M. Miri. My deepest gratitude is also extended to Dr. T. Debies from Xerox Corp. for his time and commitment to the sample analyses who, without help, this project could not be completed.

I would like to acknowledge Dr. K. S. V. Santhanam, Roberta DiLeo and Dr. B. Landi for providing the carbon nanotube samples which were key materials for the start of this Research project.

I would like to thank the Department of Chemistry at RIT for the financial support with the scholarship and teaching assistantship. Without this help I would not have the opportunity to pursue my studies in the United States.

To my friend, Wagner DaSilva, whose friendship comes since the times we were undergraduate students in Brazil. I am sincerely thankful for his guidance throughout the application process and for his advice and encouragement during my time in the M. S. Program.

My heartfelt thanks are offered to Brenda Mastrangelo for her dedication, patience and support on taking care of the necessary paperwork to comply with the academic requirements. More than just serving as an academic coordinator and advisor, I am glad to know that I also gained a sister with unconditional love and trustworthy.

My sincerest gratitude and respect is given to Dr. J. Hornak, Dr. J. Lanzafame, Mr. Thomas Allston and Ian Cawthray for the supervision, help and the professional partnership during my Teaching Assistant assignments. I thank you for trusting and respecting my work, for giving me the joy of working with you and, for all you have taught me.

I would like to thank the stockroom staff who helped me providing materials for the chemistry labs I taught or materials I needed to complete my research, Glenn, Dave, Gary, John, Paul, Rachel, Julian, and everyone else who provided me with support.

I also would like to acknowledge Lilli Jensen from the International Student Services' and Diane Ellison from the Graduate Enrollment Services' office for the academic guidance, friendship and emotional support.

To all Professors, Alpha Chi Sigma brothers and great friends I have met at RIT and in Rochester. Thank you all for the knowledge, inspiration, motivation, and friendship.

I would like to express my deepest thanks and affection to my Family and friends back home for their emotional support and words of wisdom during the difficult times of my journey. To my dad, mom, sister, brother and the doggies, my love stays with you.

Thank you all very very much for your contribution and participation in this important chapter of my life.

Abstract

Carbon nanotubes (CNTs) have many desirable bulk properties, such as, very good mechanical strength, high thermal stability, and excellent electric conductance for potential use in a variety of applications. However, their surfaces often require modification in order to achieve functionality. An important first step in the adhesion to the nanotubes is often surface oxidation. To control the metallic and semiconducting properties of CNTs, electron withdrawing halogen atoms are usually covalently bonded to the surface.

In this present Thesis, single-walled CNTs (SWCNT) powder and multi-walled CNTs (MWCNT) paper were modified with gaseous oxygen and chlorine atoms. The following investigations were performed: 1) UV photo-oxidation of MWCNT paper at room temperature and atmospheric pressure with wavelengths from low-pressure Hg lamps (λ = 253.7 and 184.9 nm) that have sufficient energy to photo-dissociate gaseous oxygen producing mainly ozone and result in chemical surface modification of the samples; 2) SWCNT powder was surface oxidized at room temperature with gaseous oxygen atoms produced by low-pressure vacuum UV (VUV) photo-oxidation (λ = 104.8 and 106.7 nm); 3) MWCNT paper and SWCNT powder were surface oxidized without the presence of radiation at room temperature with gaseous oxygen atoms produced from a microwave (MW) plasma discharge of an argon and oxygen (Ar-O_2) mixture; 4) UV photo-chlorination of MWCNT paper and SWCNT powder at room temperature with wavelengths from medium-pressure Hg lamps (centered at *ca.* 300 nm for Cl_2 at *ca.* 100 torr gas pressure) and low-pressure Hg lamps (λ = 253.7 nm and 184.9 nm for HCl at *ca.* 40 torr gas pressure) that have sufficient energy to photo-dissociate gaseous Cl_2 and HCl producing chlorine atoms and result in chemical surface modification of the samples.

The carbon-, oxygen- and chlorine-containing functional groups in the top 2 – 5 nm of the sample's surface were analyzed by X-ray photoelectron spectroscopy (XPS).

List of Figures

List of Tables

1. Introduction

In 1991, the discovery of a new material in the soot of an arc-discharge experiment caught the attention of a group of researchers [1]. The tubular structures of nanoscale diameter, called multi-walled carbon nanotubes (MWCNTs), consisted of several tens and hundreds of concentric graphitic shells of carbons with adjacent shells separation of approximately 0.34 nm [2]. Two years later, single-walled carbon nanotubes (SWCNTs) were synthesized by the use of metal catalysts in an arc-discharge experiment [3]. Due to their highly complex network and large length/diameter ratio, carbon nanotubes (CNTs) are considered to possess incredible thermal, electronic and mechanical properties. CNTs can be metallic or semiconducting depending on their structural parameters which make them attractive materials for electronic devices, and applications in nanotechnology. Also, their high Young's modulus and tensile strength make them preferable for composite materials with enhanced mechanical properties [2]. Numerous studies with these novel materials have been done to explore their applications in thermal materials [4], energy storage and power generation [5-7], sensors [8-10], superconductors [11], optics [12, 13], catalyst support [14, 15], electronics [16, 17], polymer composites [18], and medicinal chemistry [19].

Functionalization of carbon nanotubes has proved to be a key step to improve their solubility in organic solvents and aqueous solutions and reactivity with other chemical compounds in order to achieve the specific properties for some of the applications previously listed. An important first step in the adhesion of materials to CNTs is often surface oxidation [20]. For bulk processing of CNTs, many liquid-phase oxidizing agents have been utilized including: nitric acid [21-27], nitric acid/sulfuric acid

mixture [28-33], sulfuric acid/potassium permanganate mixture [30], potassium permanganate [34], sulfuric acid/hydrogen peroxide mixture [24], hydrogen peroxide [23, 24, 35, 36], and low temperature ozonolysis [37, 38]. These solution-phase oxidation methods are mild, slow, and produce a mixture of hydrogen-containing moieties associated with the –C-O-, -C=O and –COO- functional groups as observed by X-ray photoelectron spectroscopy (XPS) [27, 30, 36, 37, 39, 40].

There have been only a few studies involving gas-phase oxidation of CNTs which would eliminate the liquid waste generated from the solution-phase investigations and could be a valuable dry technique for modifying the top layers of the surface and thus, helping with the manufacture of nanoelectronic devices. High temperature gas-phase oxidation in air from 480 to 750 ºC [41, 42] and in carbon dioxide at 600 ºC [43] purifies, modifies its intrinsic structure, and improves the dispersibility of the CNT powder. XPS analysis of CNTs treated with low-pressure plasma containing Ar/O_2 or Ar/CO_2 [44] and atmospheric pressure air dielectric barrier discharge [45] shows similar oxygenated functional groups as the solution-phase results mentioned above. Gas-phase ozonolysis introduces oxygenated functionalities directly on the sidewalls and not only at the end caps of CNTs [46-49]. Use of UV radiation in air to generate O_3 *in situ* showed by TGA and Raman analyses that only *ca.* 5% of the carbons of SWCNTs were functionalized and that rapid initial oxidation occurred within 1 h of treatment which stopped after 3 h potentially due to exhaustion of active surface sites [50].

It has been mentioned previously that oxidation of CNTs helps to improve their solubility and ease of dispersion with other chemical compounds. Sidewall halogenation studies of carbon nanotubes have taken place [51] with theoretical and experimental

research of fluorinated carbon nanotubes [52] followed by bromination [53] and chlorination [52-55]. For being considered electron withdrawing groups, functionalization with halogens forms carbon-halogen bonds introducing defect sites to the sidewalls of CNTs which open a gap at the Fermi level, changing their electronic properties from metallic to semiconducting [56]. The electrical conductivity of fluorine-functionalized materials (Resistance > 20 MΩ) differs dramatically from the pristine SWCNTs (Resistance = 10-15 Ω) [57]. Halogenated CNT structures are suitable responsive materials for applications in nanoelectronic devices as well.

Following the liquid-phase oxidation methodology, most of the chlorine functionalization of CNTs has been done using liquid precursors of thionyl chloride [19, 51, 58-65], chloroform [52, 57, 59], tetrachloroethylene [52], hydrochloric acid [53], solid dichlorocarbene [51, 55, 56, 62], and very few results have been reported with reactant gases such as Cl_2 [52, 66] and $COCl_2$ [66]. The reported chlorinated functional groups attached to the CNT surface are: -CCl_2, -CCl and, -COCl as observed by: particle induced γ-ray emission (PIGE) [52], near-FTIR [62] and IR [66] spectroscopy, transmission electron (TEM) [52, 66] and atomic force (AFM) [56] microscopy, thermogravimetric analysis (TGA) [52], XPS [52, 53, 55, 66], Raman [53, 62] and energy-dispersive x-ray (EDS) [56, 62] spectroscopy.

A recent study [52] of the functionalization of SWCNTs with liquid alkyl halides such as trichloromethane and tetrachloroethylene and gaseous chlorine by ball milling at room temperature showed that this method gives functionalized samples in the range of 5.5 to 17.5 wt% of chlorine. As with oxidation studies, the amount of attached functional groups increases with increasing treatment time but after a certain time

saturation occurs. Also, liquid precursors provided higher efficiency of chlorination than gases due to more pronunciation of adsorption of liquids on the CNTs surface. The atmospheric nature of corrosive chlorine gas and the grinding in a ball mill can effectively reduce the length of the nanotubes as well as destroy their bundles [52]. A second study [66] using ball milling in gaseous atmospheres of reactant Cl_2 and $COCl_2$ introduced chloride and acyl chloride functional groups onto shortened-MWCNTs.

Modification of SWCNTs with dichlorocarbene formed from a reaction of chloroform and potassium hydroxide provided low degree of functionalization even though carbenes are well known electrophilic reagents that add to carbon-carbon double bonds [57]. Chen et al. [62] demonstrated that the reaction of soluble SWCNTs with dichlorocarbene (generated from phenyl(bromodichloromethyl)mercury) in toluene at 80 ^{o}C under argon led to functionalization of the nanotube walls with *ca.* 2 at% Cl. This saturation was sufficient to bring drastic changes in the band electronic structure of the samples brought by the covalent bond formation resulting from addition of dichlorocarbene to the wall of the soluble SWCNTs [62]. XPS experiments were performed by Lee et al. [55] to investigate surface modification of SWCNTs samples from a reaction with dichlorocarbene. Chlorine atoms amounting to about 1.6 at% were detected at the surface. The functional group –CCl was detected at a peak position of 287.7 eV in the C 1s narrow scan XPS spectrum [55]. In contrast, Hu et al. [56] reported the atomic percentage of chlorine functionalized onto SWCNTs to vary between 8% and 14% by using different amounts of dichlorocarbene precursors. Solution-phase NIR spectra showed that the intensities of both semiconducting (0.90 and 1.50 eV) and metallic transitions (2.04 eV) decreased with increasing degree of dichlorocarbene

functionalization due to the extended damage of the π-network, thereby disrupting the translational symmetry and changing the electronic structure of the SWCNTs. These interband transitions indicate that the integrity of the SWCNTs electronic structure has been disrupted by the introduction of substituents into the sidewalls of the sample [56].

Hydrothermal treatment of SWCNTs in aqueous HCl/H_2O and HBr/H_2O mixtures caused halogenation of the pristine material and proved to be an efficient method to functionalize carbon nanotubes. Samples were heated up to 250 or 500 ^oC for 24 or 114 hours. XPS experiments showed that density of chlorine and bromine was consistently around 0.4 at%. High energy components in the XPS spectrum arise from the halide coupled to the π-system of the CNTs [53].

Thionyl chloride ($SOCl_2$) treatment of CNTs produces mainly the conversion of carboxylic groups generated during the oxidative purification step of CNTs to the corresponding acyl chloride functionality (–COCl). This method has been reported as very efficient for further sample modification with amines [19, 62], diols [51], viologen units [58] and grafting of polymers [61, 63-65, 67, 68]. Parekh et al. [60], via stable room temperature post deposition functionalization, reported the improvement of the conductivity of transparent SWCNTs thin films via exposure to nitric acid and $SOCl_2$. The researchers suspected that -Cl or -COCl functional groups enhance SWCNTs transport properties thus, having beneficial effects on the conductivity of SWCNT films [60].

In this Thesis, the following gas-phase investigations were performed:

a) UV photo-oxidation of MWCNT paper at room temperature and atmospheric pressure with wavelengths from low-pressure Hg lamps

(λ = 253.7 and 184.9 nm) that have sufficient energy to photo-dissociate gaseous oxygen producing ozone and result in chemical modification of the sample's surface.

b) SWCNT powder was surface oxidized at room temperature with gaseous oxygen atoms produced by low-pressure vacuum UV (VUV) (λ = 104.8 and 106.7 nm) photo-oxidation.

c) MWCNT paper and SWCNT powder were surface oxidized without the presence of radiation at room temperature with gaseous oxygen atoms produced by microwave (MW) plasma discharge of an argon and oxygen ($Ar\text{-}O_2$) mixture.

d) UV photo-chlorination of MWCNT paper and SWCNT powder at room temperature with wavelengths from medium-pressure Hg lamps (broadband of radiation centered at *ca.* λ = 300 nm for Cl_2 at *ca.* 100 torr gas pressure) and low-pressure Hg lamps (λ = 253.7 and 184.9 nm for HCl at *ca.* 40 torr gas pressure) that have sufficient energy to produce chlorine atoms and result in chemical modification of the sample's surface.

The results of these investigations were compared to previous studies where ozone produced from high pressure, UV photo-oxidation (λ = 184.9 and 253.7 nm) and gaseous oxygen atoms produced by low-pressure VUV photo-oxidation (λ = 104.8 and 106.7 nm) were reacted with SWCNT powder [20], SWCNT paper [69], MWCNT powder [70] and MWCNT paper [71]. X-ray photoelectron spectroscopy (XPS) was the analytical technique used to detect and analyze the carbon-, oxygen- and chlorine-containing functional groups in the top 2 – 5 nm of the modified CNT's surface.

2. Experimental

2.1. SWCNT powder

The SWCNT powder (physical appearance of soot), which was purchased from Strem Chemicals, Inc., Newburyport, MA (product no. 06-0508, lot no. 84428119) consisted of tubes with diameters from 0.7 to 2 nm, lengths from 2 to 20 μm and was usually present in bundles of 20 tubes. The powder was used as received and placed within a well of diameter and depth of *ca.* 2 and 1 mm, respectively, formed in a quartz block (Figure 1) for the oxidation and chlorination experiments and XPS analysis.

Figure 1. SWCNT powder within a well formed in a quartz block.

2.2. MWCNT paper

The MWCNT paper was synthesized by the NanoPower Research Lab at the Rochester Institute of Technology using a procedure previously reported [72]. A chemical vapor deposition (CVD) reactor was constructed with a coaxial injection design. The injection tip was fabricated using quartz capillary tubing having an o.d. of 3 mm and an i.d. of 1 mm which was encased in a stainless steel jacket.

A precursor solution of cyclopentadienyl iron dicarbonyl dimer in xylene (0.08 M) was injected into the hot-zone of the furnace by a mechanical pump for consistent delivery rates. The material was synthesized at 725 ^{o}C, with an Ar flow rate of 0.75 L/min, and a precursor delivery rate of 3.5 mL/h. The as-produced MWCNT powder (physical appearance of soot, Figure 2) was dispersed in acetone, sonicated for 30 min, and filtered through a Teflon filter with 1 µm pore to form the paper. The resulting MWCNT paper (physical appearance of a tissue paper sheet, Figure 2) produced was *ca.* a 1.5 cm diameter circle with a thickness of *ca.* 10 µm (Figure 2). Characterization of the high purity MWCNTs was carried out using intensity ratios of Raman spectroscopy peaks which were consistent with SEM observations and TGA analyses [73]. SEM micrographs showed a range of tube diameters from 11 to 139 nm and an average diameter of 58 ± 4 nm at a 95% confidence level [71, 73].

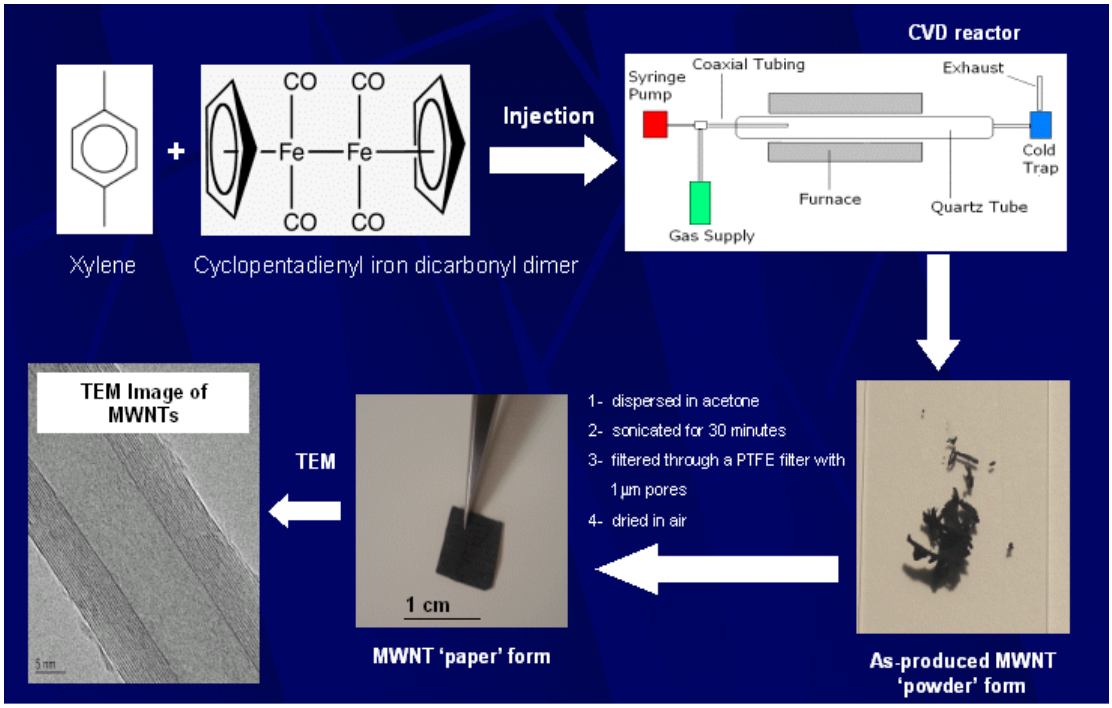

Figure 2. Processing of MWCNTs from powder to paper form [74].

The MWCNT paper was attached to the top of a microscope cover slip using a double-sided adhesive tape and subjected to the oxidation and chlorination experiments and XPS analysis.

2.3. UV photo-oxidation

A Rayonet photochemical chamber (manufactured by Southern New England Ultraviolet Co., Inc., Branford, CT) having an i.d. of 25.4 cm was equipped with 16 low-pressure Hg lamps that emit 184.9 and 253.7 nm photons with about a 1:6 intensity ratio (Figure 3). A cylindrical photochemical cell (2.54 cm diameter, 17.8 cm long) was constructed of Suprasil® quartz and fitted with a Cajon removable high vacuum stainless steel fitting to allow placement and removal of the sample from the cell [20] (Figure 4). High purity nitrogen and oxygen (99.99%) were flowed through the chamber and cell for at least 10 min at flow rates of about 5×10^3 and 43 cm^3/min, respectively, to displace air prior to the ignition of the radiation source.

Using this cell design (*i.e.*, optical path length), known photo-absorption spectra for oxygen and ozone [75, 76] and estimated concentrations of oxygen and ozone, Beer-Lambert law calculations show that a significant fraction of the UV radiation is transmitted through the reaction mixture to interact with the CNT surface.

During treatment of a sample, the exit gas was passed through a solution of saturated KI in order to remove ozone prior to emission into the hood.

Top view of UV chamber

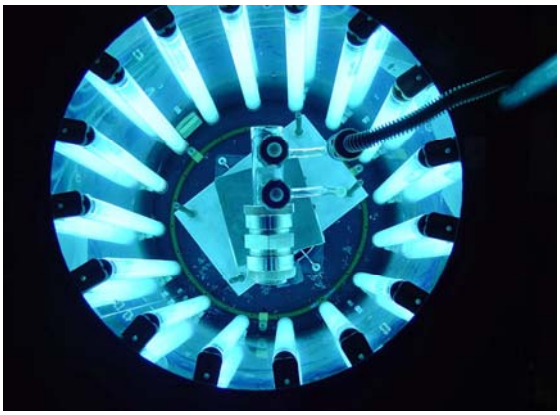

Figure 3. Rayonet photochemical reactor.

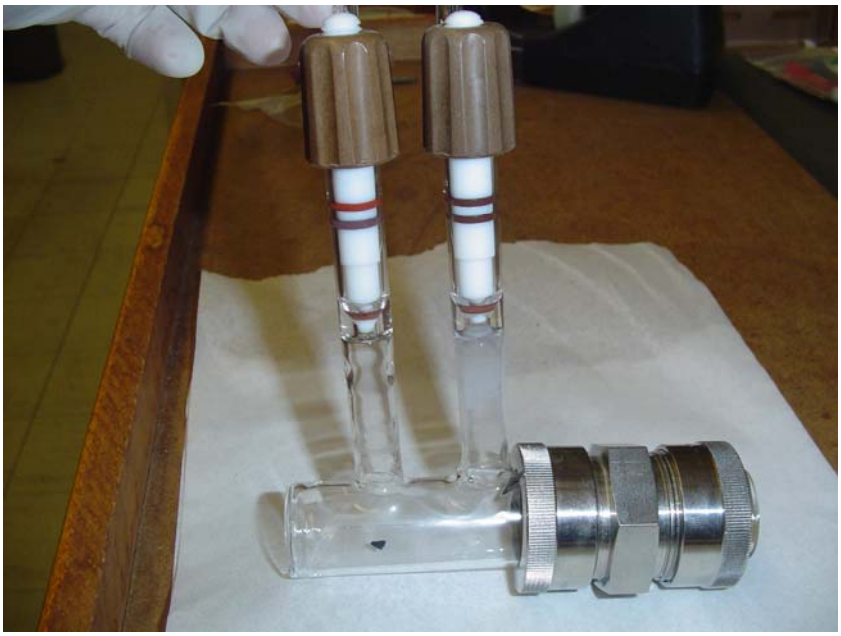

Figure 4. Quartz photochemical cell.

2.4. VUV photo-oxidation and MW plasma discharge of an Ar-O_2 mixture

Low-pressure argon MW plasmas, operating at a frequency of 2.45 GHz and absorbed power of 33 – 44 W (the difference between the forward and reflected power), and 25 – 31 W were used as the source of VUV radiation and oxygen atoms [77], respectively, to modify the surface of the samples located downstream from the plasmas.

For VUV photo-oxidation, the SWCNT powder was placed 23.8 cm downstream from the vertical MW discharge of Ar. Oxygen was introduced into the vacuum system about 3 cm above the sample. The argon and oxygen flow rates were 50 and 10 cm^3/min, respectively. The reaction chamber pressure was maintained at (4.3 - 4.8) × 10^1 Pa. At the reaction time associated with this distance, charged particles and metastables from the plasma contribute negligibly because of recombination and deactivation processes occurring in transit to the sample [77].

For the MW discharge of an Ar-O_2 mixture, the construction and operation of the discharge flow system was similar to that used in the study of the gas-phase O + HBr reaction [78]. Atomic oxygen was generated from an Ar-O_2 mixture having flow rates of 50 and 10 cm^3/min, respectively, with the pressure in the chamber at (1.2 – 4.1) Pa. The vacuum system was designed so that the horizontal discharge was located *ca.* 41 cm upstream from the SWCNT powder and MWCNT paper and the radiation from the discharge was not directed at the samples.

The reactor designs for both the VUV and MW plasma discharge experiments are displayed in Figures 5 and 6, respectively.

Figure 5. VUV reactor design (vertical plasma).

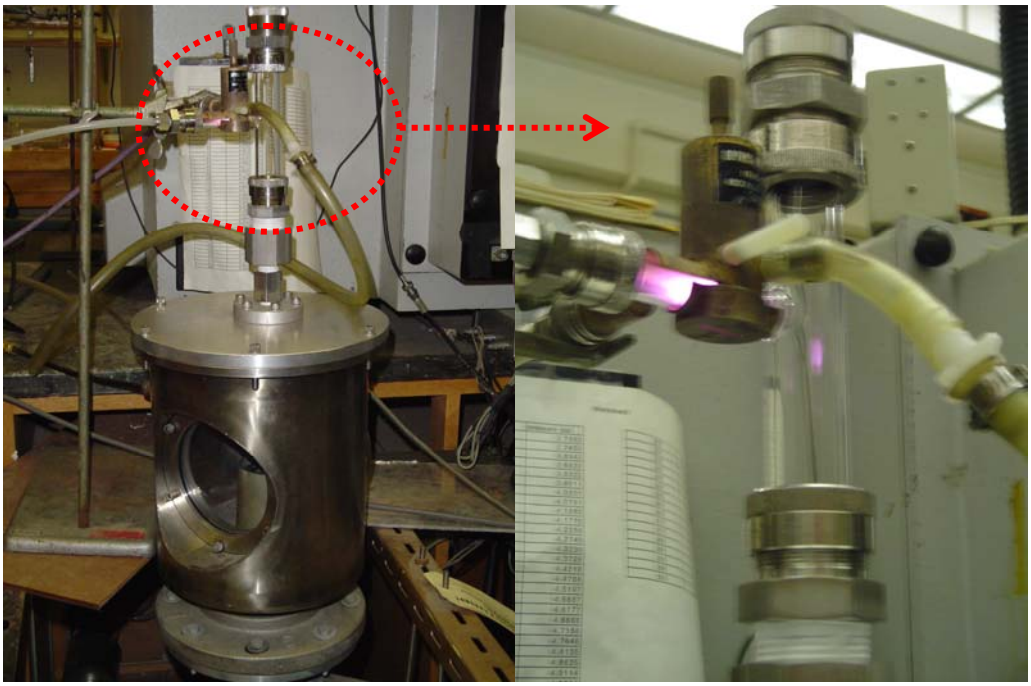

Figure 6. MW plasma discharge reactor design (horizontal plasma).

2.5. UV photo-chlorination

The same Rayonet photochemical chamber used for the UV photo-oxidation study was used for the UV photo-chlorination experiment, except that Cl_2 and HCl were the reactant gases. UV photo-chlorination experiments with Cl_2 required the use of a set of 16 medium-pressure Hg lamps (RPR-300 nm, Sunlight Phosphor), that emit a broadband of wavelengths from *ca.* 250 - 400 nm with a maximum intensity at 300 nm (Figure 7), that overlapped with the photo-absorption spectrum of gaseous chlorine [79].

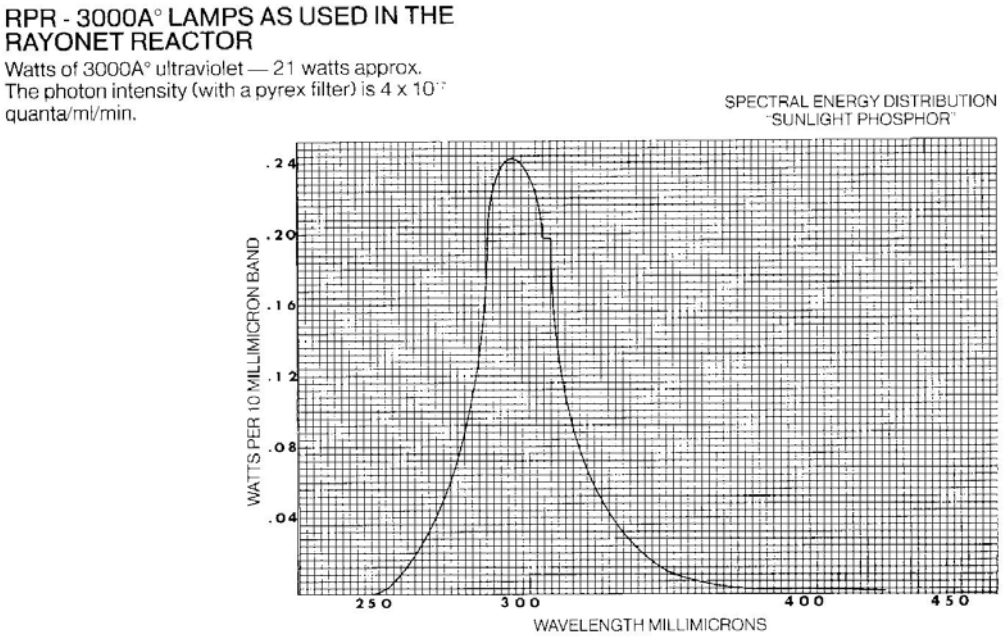

Figure 7. Spectral energy distribution for RPR-300 nm Hg lamps provided by Southern New England Ultraviolet Co., Inc., Branford, CT.

UV photo-chlorination using HCl gas required the chamber to be equipped with 16 low-pressure Hg lamps that emit 253.7 and 184.9 nm photons with about 6:1 intensity ratio. Photons of 184.9 nm have sufficient energy to break the H-Cl bond forming H and Cl atoms [79] to react with the samples. High purity nitrogen (99.99%) was flowed

through the chamber at a flow rate of 5×10^3 cm^3/min to displace air prior and during the experiment.

A vacuum line made of Pyrex connected to a vacuum pump was used to trap the reactant gases in the quartz cell containing the samples of SWCNT powder and MWCNT paper (Figures 8 and 9). The gas pressure in the cell was calculated so that *ca.* 90% of the radiation was absorbed. A Hg manometer, topped off with *ca.* 2 cm of dibutyl phthalate to prevent reaction of chlorine with the Hg, was connected to one of the vacuum line stopcocks in order to measure the pressure of the gas introduced to the cell (Figures 8 and 9). The photochemical cell was filled with $(1.0 – 1.7) \times 10^4$ Pa of ultra high purity Cl_2 (Matheson Tri-Gas, Parsippany, NJ) and $(0.8 – 1.1) \times 10^4$ Pa of technical grade (99.5%) HCl gas (Airgas, Elmira, NY). The gases were de-gassed of air using at least 2 freeze-thaw cycles at 77 K.

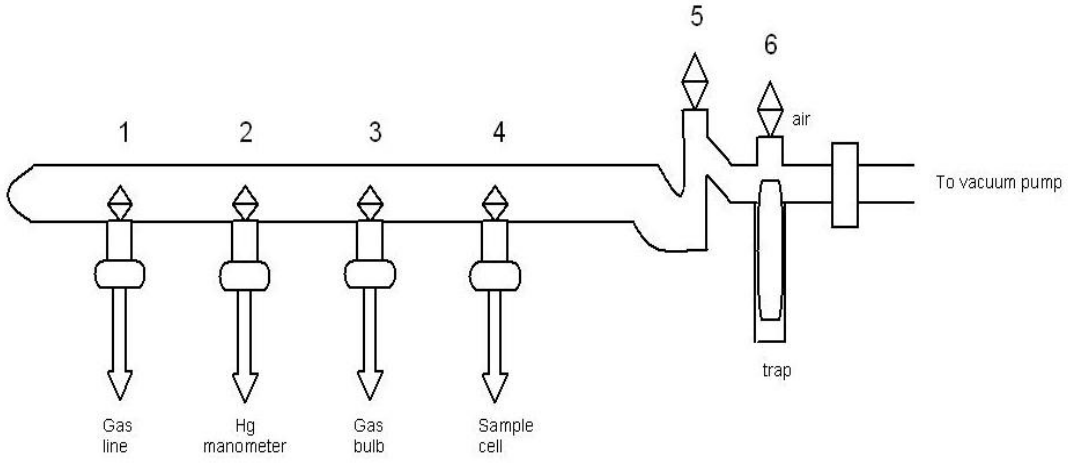

Figure 8. Vacuum line system scheme consisting of the following stopcocks, from the left to the right: 1) gas line, 2) Hg manometer, 3) gas bulb, 4) photochemical cell, 5) gas trap/vacuum pump and 6) air.

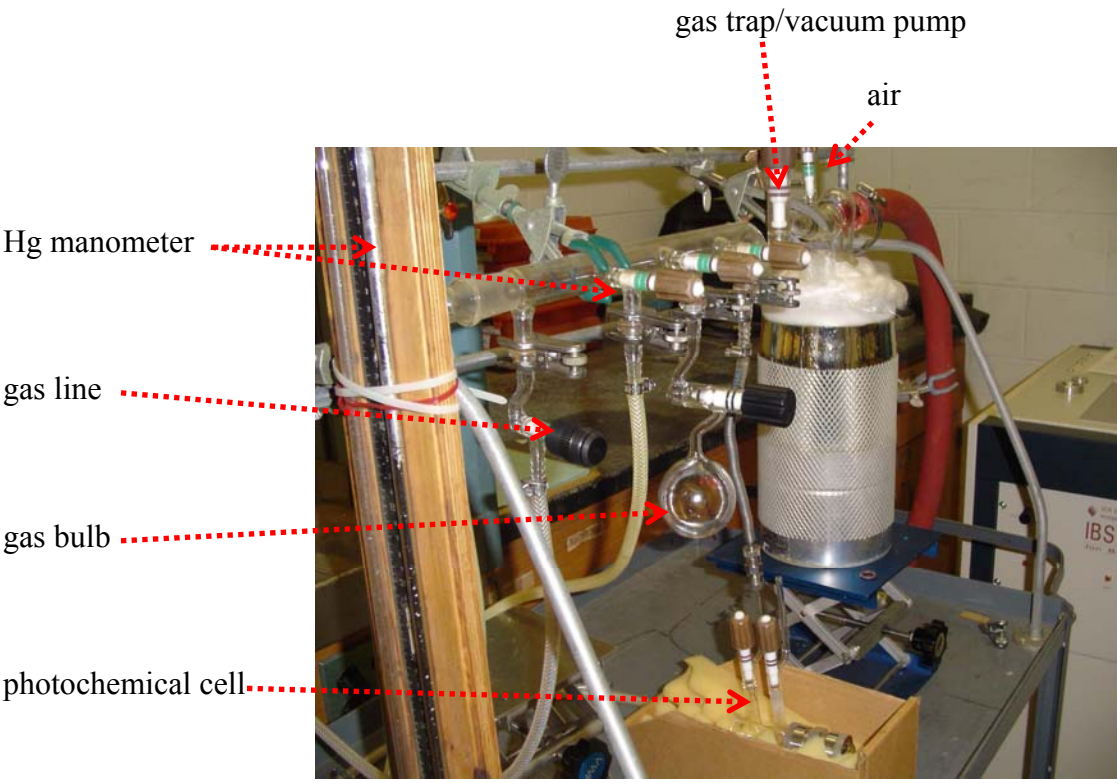

Figure 9. Vacuum line system.

Once the UV photo-chlorination treatment of the samples was completed, an extra experimental step was necessary to avoid the release of the hazardous gases into the hood. With the use of the vacuum line, the unreacted Cl_2 and HCl gases were transferred and condensed from the photochemical cell to a spare gas bulb containing 1 M NaOH solution at liquid nitrogen temperature in order to be neutralized prior to their disposal into an inorganic waste bottle.

2.6. X-ray photoelectron spectroscopy (XPS)

All samples reported in this Thesis were analyzed by XPS. XPS is a non-destructive spectroscopic technique used to analyze the top 1 – 10 nm surface chemistry

of materials [80]. To obtain the XPS spectra the material is irradiated with a source of soft X-ray beams which excite the core level electrons of the elements present on the surface of a sample. The spectrum is given as a plot of the number of core level photoelectrons detected (ordinate) versus their specific energy (abscissa), the so called binding energy given in units of electron Volts (eV). The binding energy (B. E.) of an electron is a direct measure of the required energy to remove this electron from its initial (neutral) level to the vacuum level. Since each element present on the surface possesses particular B. E. values the composition of the surface can be determined. The amount of elemental composition within the area of the irradiated material's surface is directly related to the number of detected electrons in each of the peaks of the XPS spectrum. The area under each peak is proportional to the number of atoms being present in the studied elements. By calculating the respective contribution of each peak area the composition of the chemical species on the surface can be obtained.

An XPS system is composed of a vacuumed sample chamber which contains a sample holder; a source of fixed energy radiation (soft X-ray beams) that is used to excite the core level electrons on the material's surface from their neutral to the vacuum level in order to be detected; an ultra-high vacuum environment (UHV chamber and pumps) to avoid interference of gas phase collisions with the analyses of the photo emitted electrons; an electron energy analyzer with two concentric-hemispherical magnetic field shielding that is used to disperse the photo emitted electrons according to their kinetic energy and measure their flow throughout the analyzer; and a computer/software connected to the XPS system so the surface's composition can be studied.

A Physical Electronics Model 5800 XPS system (Figure 10), located at Xerox Corp. in Webster, NY, was used to examine the top 2 – 5 nm of the sample's surface using a take-off angle of 45^{o} between the sample and the analyzer. A region of about 800 μm in diameter was analyzed. The quartz block containing the SWCNT powder (Figure 1) and/or the microscope cover slip holding the MWCNT paper were mounted directly in the XPS sample holder. The monochromatic Al Kα (1486 eV) X-ray beam irradiated the well and the electron optics of the analyzer was focused to accept only photoelectrons emitted from the nanotubes.

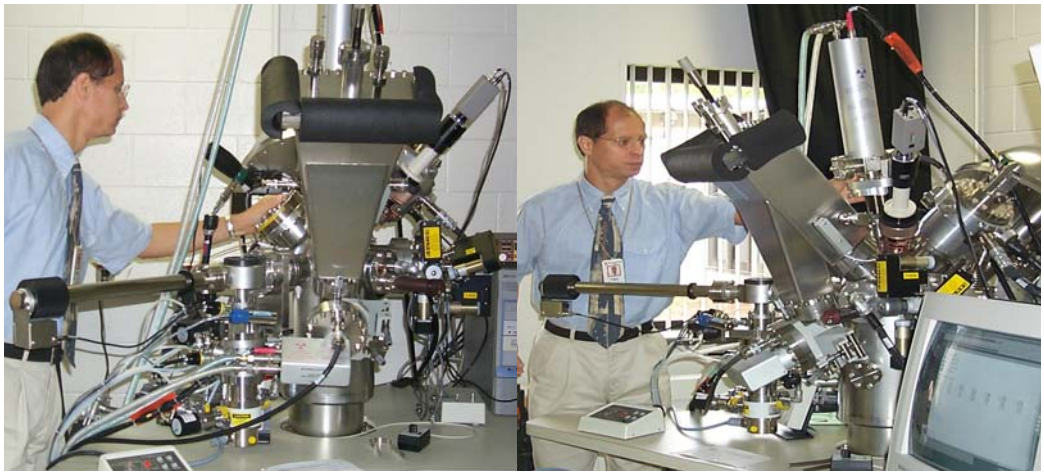

Figure 10. XPS Physical Electronics Model 5800 located at Xerox Corp. in Webster, NY.

The quantitative analyses are precise to within 5% relative for major constituents and 10% relative for minor constituents. The samples were charge-neutralized with a flood of low-energy electrons from a BaO field emission charge neutralizer. This method of analysis minimized radiation damage to the samples.

3. Results and Discussion

3.1. UV photo-oxidation of MWCNT paper

3.1.1. XPS Qualitative Analyses

The MWCNT paper contained only carbon and oxygen. No contamination was found.

3.1.2. XPS Quantitative Analyses

The quantitative analyses results for untreated and treated MWCNT paper samples are summarized in Table 1. It can be seen that the atomic percentage (at%) of carbon slightly decreased while the atomic percentage of oxygen faintly increased with treatment time. The four untreated samples contained 0.7, 0.8, 1.3 and 1.5 at% O compared to the previous measurement of 1.50 at% O reported for the MWCNT paper control of the VUV photo-oxidation study [71]. The variability in the amount of oxygen in the control samples influenced the scatter of the data observed in the treated samples. As shown in Figure 11, the saturation level of oxidation from UV photo-oxidation (2.8 ± 0.4 at% O at 95% confidence limits) was substantially lower than that observed via VUV photo-oxidation with wavelengths of 104.8 and 106.7 nm (*ca.* 7.4 at% O) [71].

Table 1. Results of XPS quantitative analyses for MWCNT paper treated with UV photo-oxidation

Sample	at% C	at% O
Untreated*	99.2	0.8
Untreated*	99.3	0.7
Untreated* (LO)	98.5	1.5
Untreated* (LO)	98.7	1.3
Treated, 20 min	98.2	1.8
Treated, 40 min	98.2	1.8
Treated, 1 h*	97.9	2.1
Treated, 1 h*	96.5	3.5
Treated, 1.5 h	96.5	3.5
Treated, 2 h*	98.0	2.0
Treated, 2 h*	97.2	2.8
Treated, 2 h* (LO)	97.7	2.3
Treated, 2.5 h (LO)	96.9	3.1
Treated, 3 h*	98.0	2.0
Treated, 3 h* (LO)	96.8	3.2
Treated, 3.5 h (LO)	96.3	3.7
Treated, 4 h (LO)	97.8	2.2

* Replicate samples

(LO) My contribution to the research.

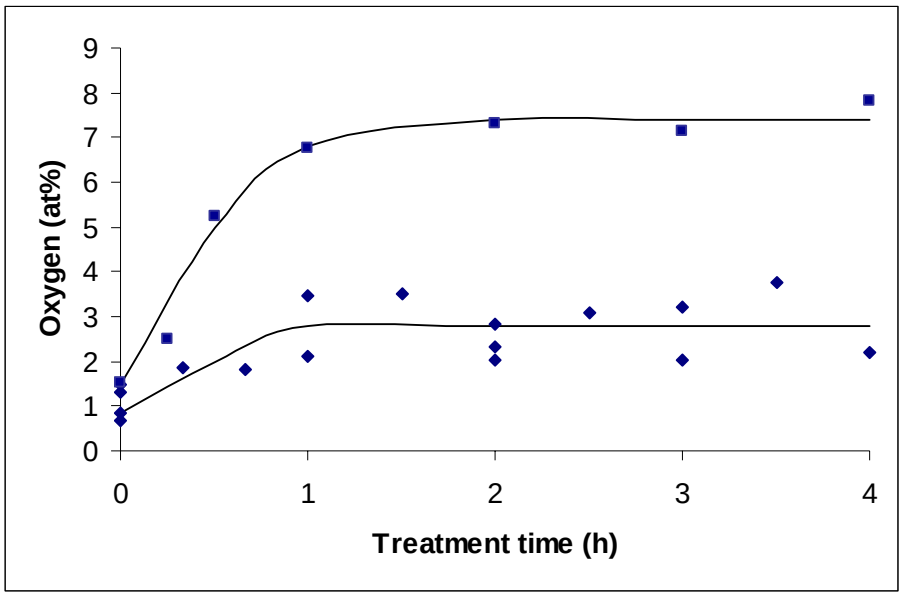

Figure 11. Plot of atomic percent of oxygen for untreated and treated MWCNT paper as a function of exposure time to UV (◆) [20] and VUV photo-oxidation (■) [71].

3.1.3. XPS Chemical State Analyses

Because of the low levels of carbon-oxygen bonding (Table 1, Figure 11), the resolution of the C 1s and O 1s spectra for the control and treated samples of MWCNT paper were very low. The saturation level of only 2.8 at% O makes it difficult to detect changes in oxidation of the treated samples from the control C 1s spectrum thus, the XPS C 1s spectrum and curve fit were not obtained for this study.

Gas-phase UV photo-oxidation of MWCNT paper with 184.9 and 253.7 nm radiation lamps resulted in an increase in oxidation of the top 2 – 5 nm of the surface (Table 1, Figure 11). However, the achieved saturation level of 2.8 ± 0.4 at% O within

approximately 60 min of treatment did not achieve a high at% O difference from the four untreated samples in Table 1 (0.7, 0.8, 1.3 and 1.5 at% O).

Molecular nitrogen is transparent to the UV radiation while ground state oxygen molecules, $O_2(^3\sum_g^-)$, in the photochemical cell absorb 184.9 nm photons [75] which have sufficient energy to break the molecular bond to form two ground state $O(^3P)$ atoms as shown in reaction (1) with its threshold wavelength [79]:

$$O_2 + h\nu \rightarrow O(^3P) + O(^3P) \qquad \lambda \leq 242.4 \text{ nm} \qquad (1)$$

Ozone, which is formed in the photochemical cell by reaction (2) involving a stabilizing molecule (M), absorbs photons from the low-pressure Hg lamps that are energetic enough to photo-dissociate ozone to produce reactive electronically-excited oxygen atoms, $O(^1D)$ and $O(^1S)$, and oxygen molecules ($O_2(^3\sum_u^-)$, $O_2(^1\Delta_g)$, $O_2(^1\sum_g^+)$) [81].

$$O(^3P) + O_2 + M \rightarrow O_3 + M \qquad (2)$$

Oxygen atoms are also formed by the photo-dissociation of ozone [81]. Both ozone [76] and oxygen atoms [82] are well known to oxidize by adding across unsaturated sp^2 carbon bonds to form an oxidized moiety (epoxy group) as has been observed in the oxidation of graphite [83, 84]. Although, the XPS C 1s spectra and curve fit for this study were not obtained, it is believed that the oxygenated moieties present on the surface of the MWCNT paper samples after UV treatment are similar to those detected for UV photo-oxidation studies of SWCNT powder [20], SWCNT paper [69] and MWCNT powder [70]. Curve fittings of the XPS C 1s spectra of these samples revealed mainly C-O-C as ether and/or epoxy functional groups, with the presence of C=O, O-C=O, O=C=O-C=O and/or O-(C=O)-O. The mechanism of reaction starts with

ozone adding across the CNTs double bond to produce a primary unstable ozonide that undergoes bond cleavage to form a carbonyl (C=O) containing compound and a Criegee intermediate [37, 46, 76]. One of the mechanisms for decomposition of the Criegee intermediate results in the formation of ester groups (O-C=O) as illustrated in Figure 12 below.

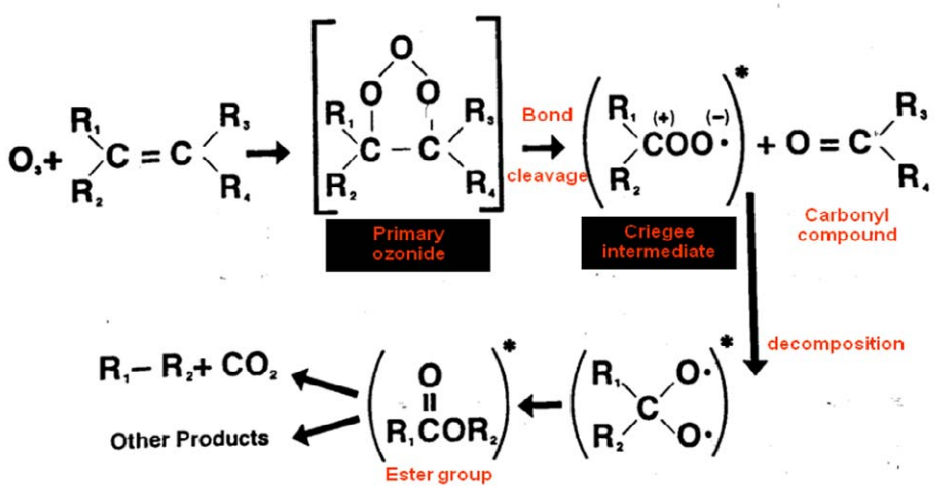

Figure 12. Mechanism of reaction of ozone with sp^2-hybridized carbon to form the Criegee intermediate [76].

UV photo-oxidation studies of SWCNT powder [20] and SWCNT paper [69] resulted in oxygen concentrations of up 23.5 and 25.5 at%, respectively. A more rapid initial rate of oxidation was observed for SWCNT powder than SWCNT paper [20]. These results may be due to the larger surface area for the powder relative to the paper as was also the case for the higher levels of oxidation found for UV photo-oxidized MWCNT powder (6 - 7 at% O) [70] compared to UV photo-oxidized MWCNT paper in this present Thesis (2.8 ± 0.4 at% O). The oxygen concentrations for UV photo-oxidized SWCNT powder [20] and paper [69] were higher relative to those observed for MWCNT

paper (Table 1) and MWCNT powder [70] potentially due to the enhanced oxidation associated with the greater curvature (*i.e.*, strain) of the smaller diameter of single shell tubes than the outer shells of multi-walled tubes [85]. Smaller diameter tubes have been reported to be more rapidly oxidized than larger diameter tubes with high temperature air [86, 87] and ozone [88].

By comparing the levels of oxidation of MWCNT paper treated with UV and VUV photo-oxidation [71] (Figure 11), a lower oxygen concentration for MWCNT paper using UV photo-oxidation (2.8 ± 0.4 at% O) is observed than that via VUV photo-oxidation with wavelengths of 104.8 and 106.7 nm (*ca.* 7.4 at% O) [71]. The presence of ozone, which is primarily formed at atmospheric pressure by UV radiation, apparently reacts more slowly than oxygen atoms, which are predominantly produced with low-pressure ((4.2 – 4.6) x 10^1 Pa), and VUV radiation [71]. The VUV photons have sufficient energy to break carbon-carbon bonds, as well as produce ground state, $O(^3P)$, and excited, $O(^1D)$ and $O(^1S)$, oxygen atoms [71] and thus, generate epoxide- and carbonyl-containing compounds from the addition of $O(^3P)$ atoms to sp^2-hybridized carbon [82].

3.2. VUV photo-oxidation of SWCNT powder

3.2.1. XPS Qualitative Analyses

The powdered SWCNT control samples only contained carbon and oxygen, while the samples treated for 1.5, 2.5, 3.5, 10, 20, 30, 40 and 90 minutes contained

carbon, oxygen and cobalt. The sample treated for 60 minutes contained carbon, oxygen, cobalt, nitrogen and silicon. Cobalt, nitrogen and silicon are impurities originated potentially from sample's synthesis, air and saliva, respectively.

3.2.2. XPS Quantitative Analyses

Table 2 summarizes the quantitative analyses results for untreated and treated SWCNT powder.

Table 2. Results of XPS quantitative analyses for VUV photo-oxidation of SWCNT powder

Sample	at% C	at% O	at% Co	at% N	at% Si
Control (untreated)*	94.9	5.2	---	---	---
6A, Control (untreated)*	95.0	5.0	---	---	---
10A, Control (untreated)*	96.1	3.9	---	---	---
6B, Treated, 1.5 min	84.6	14.8	0.6	---	---
6C, Treated, 2.5 min	83.9	15.2	0. 9	---	---
6D, Treated, 3.5 min	81.5	17.9	0.6	---	---
Treated, 10 min	80.6	19.0	0.5	---	---
10E, Treated, 20 min	78.4	21.5	0.1	---	---
10D, Treated, 30 min	78.0	21.9	0.1	---	---
10C, Treated, 40 min	80.4	19.5	0.1	---	---
Treated, 60 min	73.7	24.5	0.4	0.6	0.7
10B, Treated, 90 min	76.8	22.9	0.3	---	---

* Replicate samples

Quantitative XPS analyses of three untreated samples of SWCNT powder (Table 2) showed only the presence of carbon and oxygen with an atomic percentage (at%) for oxygen of 4.7 ± 0.7 which is in good agreement with our previously reported SWCNT powder control of 4.9 at% O [20]. Occasionally, after treatment, small amounts of Co, N and Si were detected.

Figure 13 compares the at% O results as a function of treatment time for VUV photo-oxidation of SWCNT powder with those previously reported for the UV photo-oxidation of SWCNT powder [20] and SWCNT paper [69]. Surface oxidation rapidly occurs to reach a common level of saturation using the two different treatment methods and two different forms of SWCNTs.

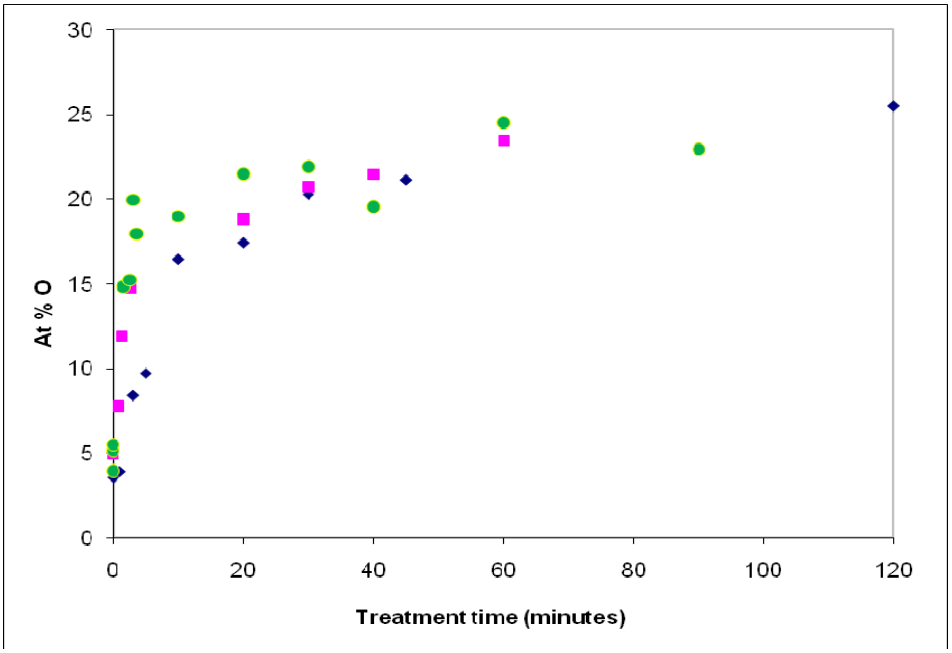

Figure 13. Plot of at% O as a function of treatment time for SWCNT powder treated with: VUV (●) and UV (■) photo-oxidation [20], and SWCNT paper treated with UV (♦) photo-oxidation [69].

3.2.3. XPS Chemical State Analyses

Figure 14 shows the results of the curve fitting for the C 1s peak of the SWCNT powder sample treated for 60 min with VUV photo-oxidation since this sample showed the highest oxygen concentration of 24.5 at% O.

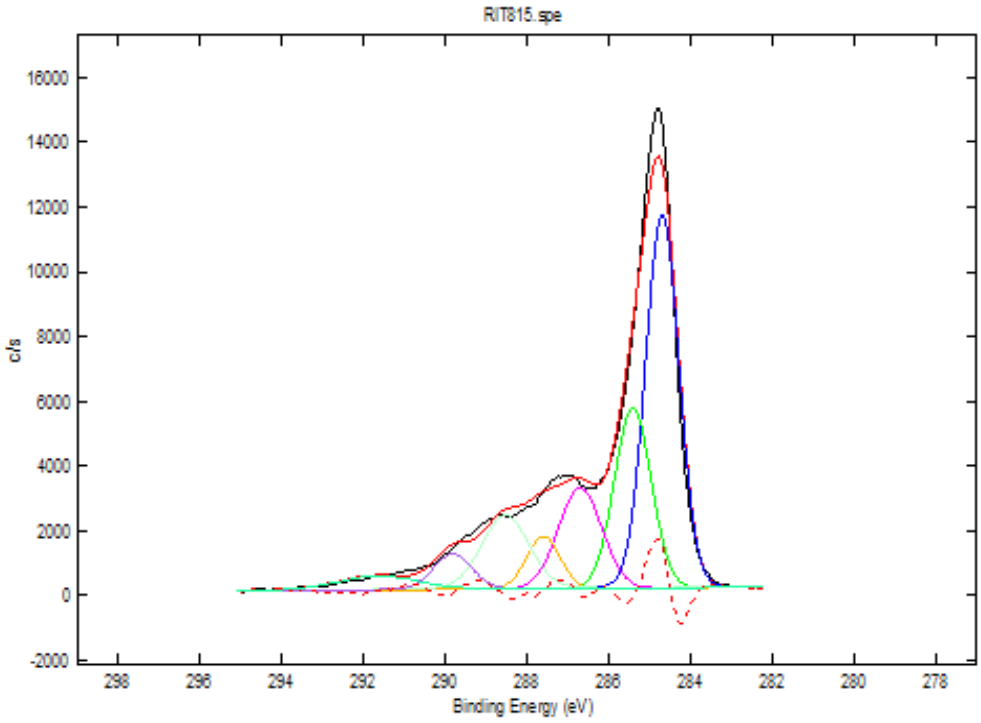

Figure 14. Results of the curve fitting for the C 1s peak of the SWCNT powder exposed to VUV photo-oxidation for 60 min.

The overlapped C 1s spectra for the control and SWCNT powder sample treated for 60 min with VUV photo-oxidation are presented and compared with the 60 min sample of the UV photo-oxidation study [20] in Figure 15. The principal peak due to sp^2 carbon-carbon bond at 284.8 eV dominates the spectra in Figures 14 and 15, but complex spectral features due to carbon-oxygen bonds are evident at higher binding energies.

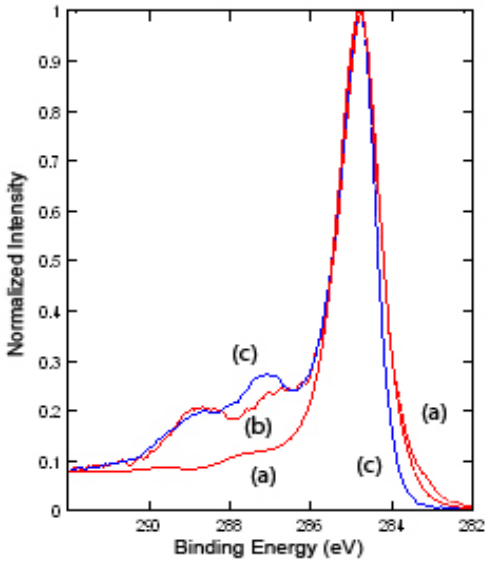

Figure 15. C 1s XPS spectra for SWCNT powder: (a) untreated, and treated for (b) 60 min with UV photo-oxidation [20] and (c) 60 min with VUV photo-oxidation.

Table 3 shows the XPS C 1s curve fitting completed for the powdered SWCNT control and samples treated for 60 min with VUV (Figure 14) and UV photo-oxidation [20]. Binding energy (B. E.) values reported in the literature [89] were utilized to assign the following peaks with increasing binding energy: C-C sp^2, C-C sp^3, C-O-C as ether and/or epoxy, C=O, O-C=O, O=C-O-C=O and/or O-(C=O)-O. The C 1s binding energy at 289.8 eV for the anhydride group, O=C-O-C=O [89], has been reported to have similar values as the carbonate-like, O-(C=O)-O, moiety [90]. As a result of the variety of species and similar contributions, the high binding energy region of the spectra has a broad undulating appearance. The peaks were modeled with different full width at half maximum by assignment. The C 1s peaks due to carbon-carbon bonding were fit with peaks whose full width at half maximum was about 0.7 eV while the peak due to energy loss was fit with a peak with a full width at half maximum of 1.8 eV. The energy loss

peak is correspondent to electrons originated from below the surface that suffered energy loss through collisions and were unable to make it out of the surface, or they escaped the surface with considerable energy loss. The percentage of carbon species was estimated by curve fitting the minimum number of peaks necessary to achieve chi-squared values of 2.0 or less. The absolute percentages of carbon were calculated by multiplying the C at% from the quantitative analyses times the percent contribution from the species obtained from the curve fitting. Therefore, the sum of the carbon concentrations in Table 3 equals the concentration of carbon obtained from the quantitative analyses and not 100%.

Table 3. Results of absolute % of C-containing groups for control SWCNT powder and samples treated for 60 min with VUV and UV [20] photo-oxidation

Assignment	**B. E. (eV)**	**Untreated, (6A)**	**VUV, 60 min**	**UV, 60 min [20]**
C-C sp^2	284.7	48.3	29.5	28.1
C-C sp^3	285.1	28.5	15.5	19.8
C-O-C, 	286.0	3.9	9.6	6.8
C=O	287.0	4.8	4.4	9.1
O-C=O	288.6	3.8	8.8	6.8
O=C-O-C=O, O-(C=O)-O	289.8	2.8	3.7	3.8
Energy Loss	292.0	2.9	2.2	1.5
Total =		95.0	73.7	75.9

Equation (3) below shows the radiation emitted from excited Ar atoms produced by low-pressure MW discharge:

$$Ar^* \rightarrow Ar + h\nu \qquad (3)$$

Neutral atomic resonance lines, arising from $^3P_1 \rightarrow {}^1S_0$ and $^3P_2 \rightarrow {}^1S_0$ transitions occur at 104.8 and 106.7 nm for Ar, respectively [91]. Oxygen molecules absorb in the VUV region of the electromagnetic spectrum [75]. The photochemical steps shown in equations (1), (4) and (5) produce ground, ^3P, and electronically excited, ^1D and ^1S, oxygen atoms [79] respectively. Thus, these steps are energetically possible using the Ar MW source.

$$O_2 + h\nu \rightarrow O(^3P) + O(^1D) \qquad \lambda \leq 175 \text{ nm} \qquad (4)$$

$$O_2 + h\nu \rightarrow O(^3P) + O(^1S) \qquad \lambda \leq 133.2 \text{ nm} \qquad (5)$$

Table 3 also reports the absolute carbon percentages for the VUV photo-oxidation experiments compared to the UV photo-oxidation [20] technique. In contrast to the UV experiment, the presence of VUV photons (11.6 and 11.8 eV), which have sufficient energy to readily break carbon-carbon bonds (*ca.* 3 eV) and potentially form excited oxygen atoms, produce more of the C-O-C (as ether and/or epoxy) and O-C=O functional groups than the C=O moiety mostly present in the UV experiment [77].

Figure 16 shows the proposed mechanism of reaction of oxygen atoms with the sp^2-hybridized carbon bond [82] in the VUV experiment which formed mostly the C-O-C moiety (as ether and/or epoxy) and Figure 17 [20] shows the mechanism of reaction of O_2 with the biradical intermediate to form the carbonyl moiety (C=O).

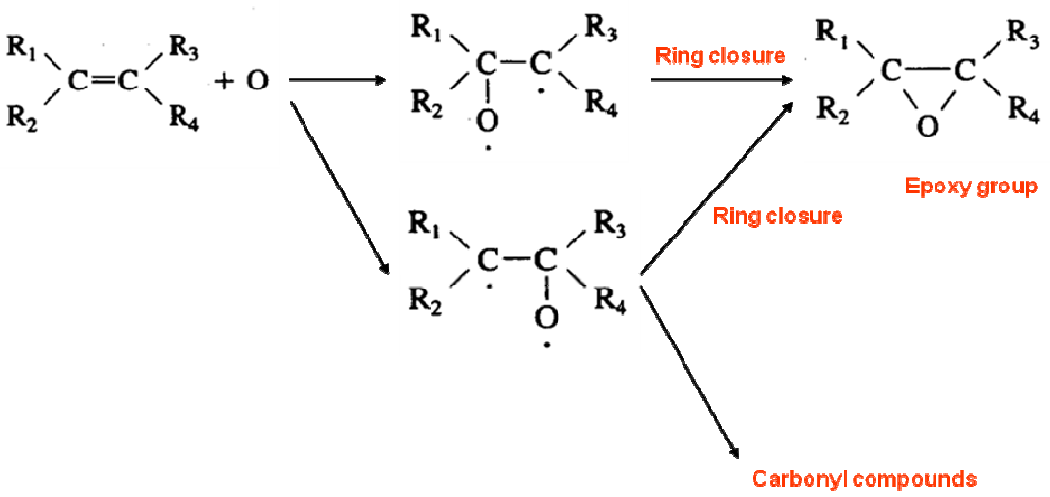

Figure 16. Reaction of O atom with the sp^2-hybridized carbon bond [82] to form the C-O-C (as ether and/or epoxy) functional group.

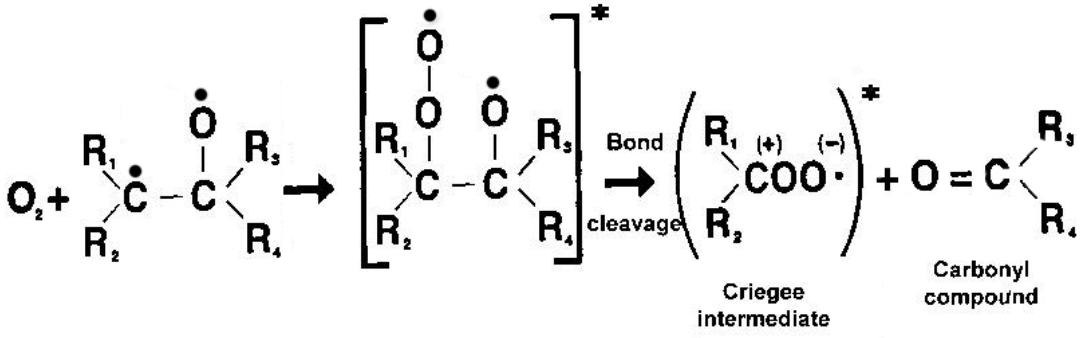

Figure 17. Reaction of O_2 with a biradical intermediate to form the C=O (carbonyl) functional group [20].

The reaction of VUV-produced oxygen atoms with SWCNT powder resulted in *ca.* 24 at% O (Table 2, Figure 13). A similar level of oxidation was obtained for the reaction of UV-produced ozone with SWCNT powder (23.5 at% O) [20]. As shown in Table 1, Figure 11, the saturation level resulting from UV photo-oxidation of MWCNT paper was *ca.* 2.8 at% O compared to *ca.* 7.4 at% O for VUV photo-oxidation (Figure 11)

[71]. The greater curvature (*i.e.*, strain) on the smaller diameter of SWCNTs possibly accounts for their increased reactivity relative to the larger diameter outer shells of the MWCNTs.

3.3. Treatment of SWCNT powder and MWCNT paper using a MW plasma discharge of an Ar-O_2 mixture

3.3.1. XPS Qualitative Analyses

3.3.1.1. SWCNT powder

The control and powdered SWCNT samples contained carbon and oxygen. The SWCNT treated for 60 min contained also nitrogen.

3.3.1.2. MWCNT paper

The MWCNT paper samples contained only carbon and oxygen. No contamination was found on these samples.

3.3.2. XPS Quantitative Analyses

3.3.2.1. SWCNT powder

Table 4 summarizes the quantitative analyses results for untreated and treated SWCNT powder. The untreated sample (18A) contained 4.7 at% O which is in good

agreement with previous measurements of 4.9 at% O [20]. Within 2 min of treatment, the oxygen concentration more than doubled (10.8 at%) relative to the control (4.7 at%). The amount of oxygen on the sample's surface increased with increasing time of exposure up to 60 – 120 min where a plateau value is reached at *ca.* 16.4 at% O.

Table 4. Results of XPS quantitative analyses of SWCNT powder oxidized by oxygen atoms produced from a MW discharge of an Ar-O_2 mixture

Sample	at% C	at% O	at% N
18A, Control (untreated)	95.3	4.7	0.0
18D, Treated, 2 min	89.2	10.8	0.0
18F, Treated, 5 min	88.0	12.0	0.0
18G, Treated, 10 min	84.6	15.4	0.0
18H, Treated, 17 min	85.7	14.3	0.0
18I, Treated, 20 min	85.8	14.2	0.0
18J, Treated, 30 min	85.4	14.6	0.0
18K, Treated, 45 min	84.5	15.6	0.0
18B, Treated, 60 min	82.0	17.0	1.0
18C, Treated, 90 min	84.2	15.8	0.0
18E, Treated, 120 min	83.5	16.5	0.0

3.3.2.2. MWCNT paper

Table 5 summarizes the quantitative analyses results for untreated and treated MWCNT paper. The untreated sample (20A) contained 1.7 at% O which is in good agreement with previous measurements of MWCNT paper controls for UV (Table 1) and

VUV photo-oxidation studies (1.5 at% O) [71]. The initial 10 min of treatment had no significant effect upon the surface chemistry of the nanotubes. After 15 min of treatment, a definite increase in the concentration of oxygen was observed. A plateau value of *ca.* 6.3 at% O is reached with increasing time of exposure up to 60 – 90 min.

Table 5. Results of XPS quantitative analyses of MWCNT paper oxidized by oxygen atoms produced from a MW discharge of an Ar-O_2 mixture

Sample	at% C	at% O
20A, Control (untreated)	98.3	1.7
20B, Treated, 2 min	97.9	2.1
20C, Treated, 5 min	98.0	2.0
20D, Treated, 10 min	97.8	2.2
20E, Treated, 15 min	95.7	4.4
20F, Treated, 20 min	95.0	5.0
20H, Treated, 45 min	94.3	5.7
20I, Treated, 60 min	93.7	6.3
20J, Treated, 90 min	93.7	6.3

Figure 18 shows the plot of oxygen concentration in units of atomic percent versus treatment time in minutes of SWCNT powder compared to MWCNT paper for the MW discharge experiments. This method provided an increase in the amount of oxygen concentration on the sample's surface reaching saturation levels of oxidation after 1 hour of treatment. As with the UV and VUV photo-oxidation studies, MW discharge experiments produced higher atomic concentration of oxygen (*ca.* 16.4 at%) for SWCNT

powder than for MWCNT paper (*ca.* 6.3 at%). The larger diameter of the outer shell of the MWCNTs possibly accounts for their decreased reactivity relative to the smaller diameter SWCNTs which possess greater curvature (*i.e.*, strain).

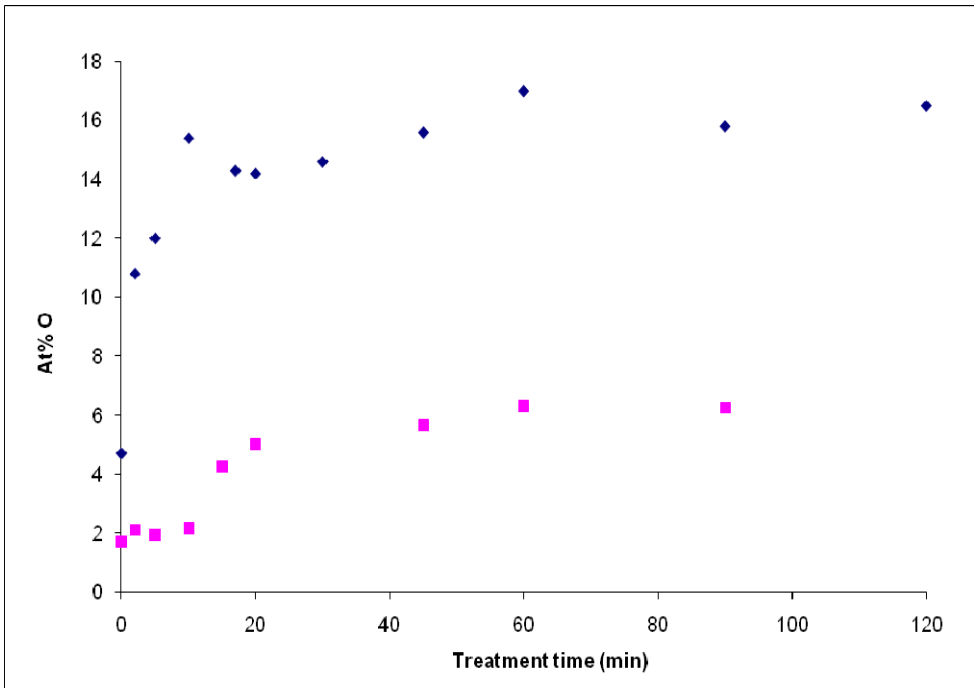

Figure 18. Plot of atomic percent of oxygen as a function of treatment time for SWCNT powder (♦) and MWCNT paper (■) samples treated by the MW discharge method which produces oxygen atoms.

Figure 19 shows that the SWCNTs treated downstream from the MW of an Ar-O_2 mixture in the absence of photons contained lower levels of oxidized species (*ca.* 16.4 at% O) than the nanotubes exposed to VUV and UV [20] photo-oxidation (*ca.* 24 at% O). The level of oxidation obtained by the MW discharge of a 5:1 mixture of Ar:O_2 are in good agreement with those reported when carbon nano-fibers/tubes are

treated with 27.12 MHz RF discharges containing 1:1 mixtures of Ar:O_2 [44, 92] and pure O_2 [93].

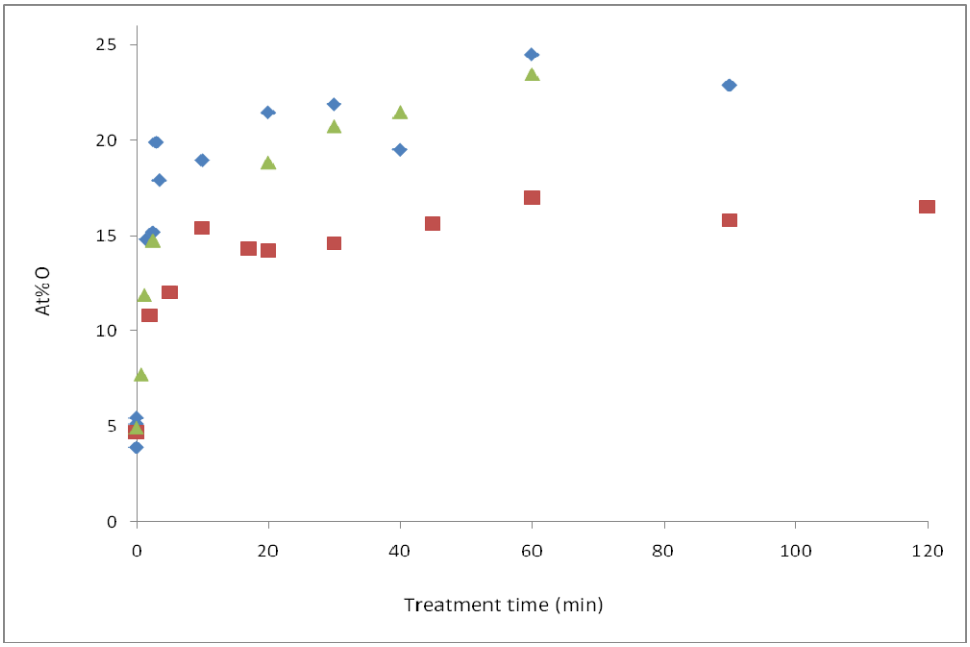

Figure 19. Plot of atomic percent of oxygen as a function of treatment time for SWCNT powder treated with VUV (♦) and UV (▲) photo-oxidation [20] and the MW discharge method which produces oxygen atoms (■).

Figure 20 shows the plot of oxygen concentration in units of atomic percent versus treatment time in minutes for MWCNT paper treated with O atoms in the presence (VUV) [71] and absence (MW discharge of an Ar-O_2 mixture) of radiation. There is a small difference in the oxygen atom saturation level of *ca.* 7.4 at% O for the VUV-treated MWCNT paper [71] compared to *ca.* 6.3 at% O detected on the MWCNT paper's surface using the MW discharge method without radiation. The scatter in the data at short treatment times is potentially due to the variability in the at% O observed for the untreated samples.

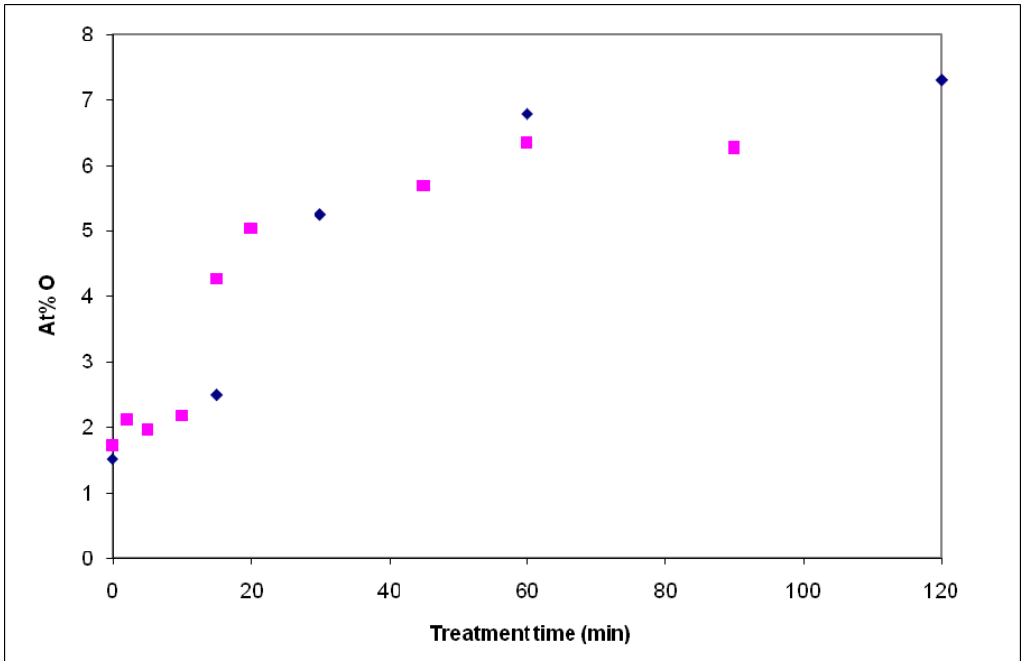

Figure 20. Plot of atomic percent of oxygen as a function of treatment time for MWCNT paper treated with oxygen atoms in the absence (■) and presence (♦) [71] of radiation.

3.3.3. XPS Chemical State Analyses

3.3.3.1. SWCNT powder

The overlapped C 1s spectra for the control and powdered SWCNT samples treated from 2 to 120 min (samples Series 18A-18K in Table 4) with O atoms produced from the MW discharge method are presented in Figure 21. The principal peak due to sp^2 carbon-carbon bonding at 284.8 eV dominates the spectra, but complex spectral features due to carbon-oxygen bonding are evident at higher binding energies (from 286 to 290 eV).

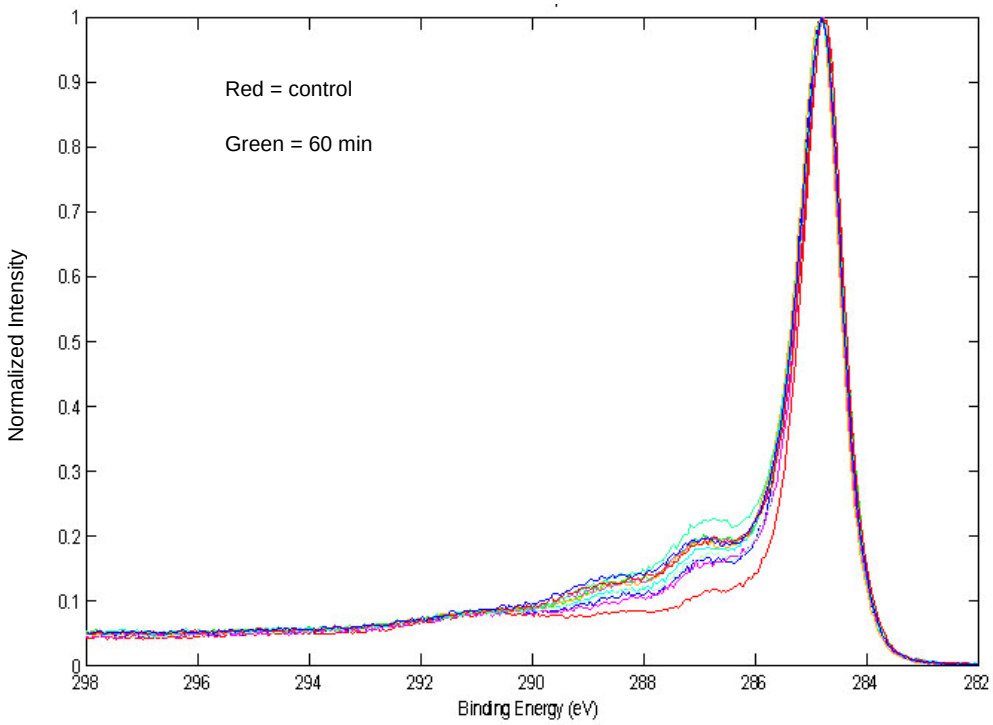

Figure 21. XPS overlapped C 1s spectra for control and powdered SWCNT samples treated from 2 to 120 min with O atoms produced from the MW discharge method.

Binding energy (B. E.) values reported in the literature [89] were utilized to assign the peaks with increasing binding energy and determine the absolute percentage of carbon. Curve fitting was completed for the XPS C 1s spectra for the control and powdered SWCNT sample treated for 1 h with oxygen atoms produced from the MW discharge of an Ar-O_2 mixture using the same methodology previously described in section 3.2.3. The binding energies, peak assignments and absolute percentages of carbon are reported in Table 6.

Table 6. Results of absolute % of C-containing groups for control (18A) and powdered SWCNT sample treated for 60 min (18B) with oxygen atoms produced from a MW discharge of an Ar-O_2 mixture

Assignment	B. E. (eV)	Untreated (18A)	Treated, 60 min (18B)
C-C sp^2	284.7	57.1	37.7
C-C sp^3	285.1	16.2	20.5
C-O-C, 	286.0	5.7	5.7
C=O	287.0	4.8	8.2
O-C=O	288.6	2.9	4.1
O=C-O-C=O, O-(C=O)-O	289.8	1.9	3.3
Energy Loss	292.0	6.7	2.5
Total =		95.3	82.0

There is a decrease in the amount of carbon and an increase in the amount of oxygen with increasing treatment time showing that this method was effective for introducing oxygen-containing moieties onto the surface of the samples.

Comparing this data with those from Table 3, treatment of SWCNT powder using MW discharge of an Ar-O_2 mixture and UV photo-oxidation [20] showed to originate more of the carbonyl (C=O) functional groups than the C-O-C (as ether and/or epoxy) and O-C=O moieties mostly generated by the presence of VUV photons and O atoms [77].

3.3.3.2. MWCNT paper

As shown in Figure 22, the principal peak of the overlapped C 1s spectra for the MWCNT paper functionalized by the MW discharge method at 284.8 eV is dominant due to sp^2 carbon-carbon bonding. Besides a steady increase on the shoulder (286 eV) of the sp^3-hybridized C 1s peak indicating the presence of complex spectral features due to C-O bonding for treatment times ranging from 0 to 90 min, the overlapped C 1s spectra for these samples virtually did not change with treatment due to the low concentration of oxygen on the surface (*ca.* 6.3 at% O).

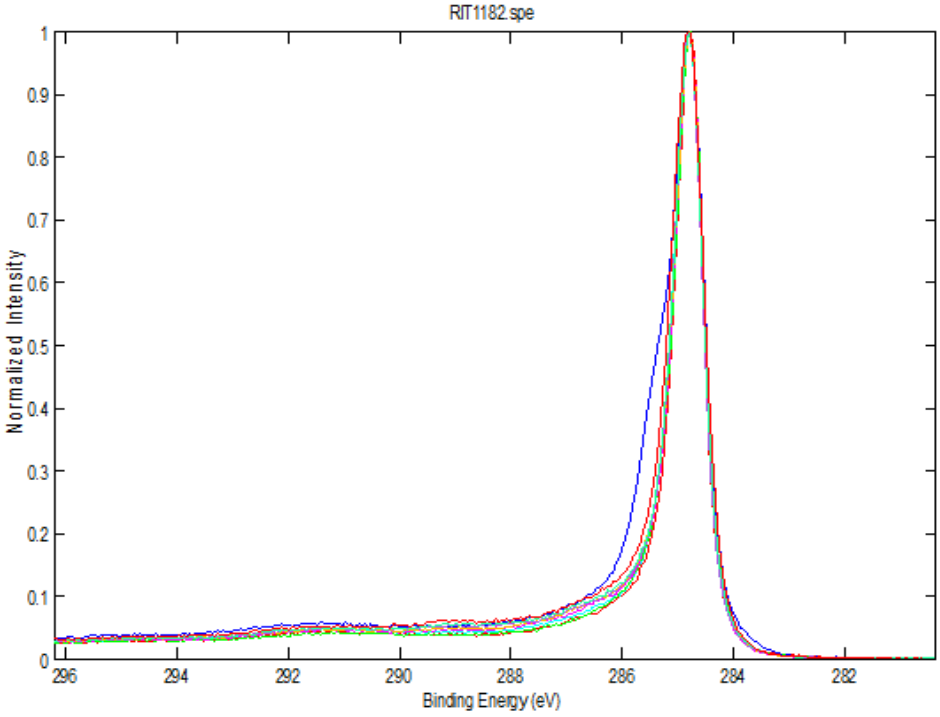

Figure 22. Overlapped C 1s XPS spectra for control MWCNT paper and samples treated up to 90 min with O atoms produced from a MW discharge of an Ar-O_2 mixture.

Curve fits for the C 1s spectra were completed in order to determine the binding energies, peak assignments and absolute percentages of carbon. The methodology

employed was the same as previously described in section 3.2.3. Table 7 summarizes the results of the curve fitting for the MW discharge experiments of the control (sample 20A in Table 5) and 90 min (20J) treated MWCNT paper samples. The curve fitting indicates that treatment resulted in the increases of the C-O-C, C=O, O-C=O, O=C-O-C=O and/or O-(C=O)-O moieties. The changes in the moieties' concentration resulted in the slight increases observed for the concentration of oxygen.

Table 7. Results of absolute % of C-containing groups for control (20A) MWCNT paper and sample treated for 90 min (20J) with oxygen atoms produced from a MW discharge of an Ar-O_2 mixture

Assignment	**B. E. (eV)**	**Untreated (20A)**	**Treated, 90 min (20J)**
C-C sp^2	284.8	65.3	57.5
C-C sp^3	285.2	17.9	12.8
C-O-C, 	286.2	2.1	6.7
Energy Loss	286.5	2.0	1.9
C=O	287.2	1.0	3.4
Energy Loss	287.7	1.8	1.4
O-C=O	288.6	1.5	2.3
O=C-O-C=O, O-(C=O)-O	289.3	2.5	3.2
Energy Loss	290.8	2.1	2.8
Energy Loss	292.2	2.4	2.4
		Total = 98.3	Total = 93.7

3.4. UV photo-chlorination of MWCNT paper and SWCNT powder with Cl_2 gas

3.4.1. MWCNT paper

3.4.1.1. XPS Qualitative Analyses

The control MWCNT paper contained only carbon and oxygen. The treated samples contained carbon, oxygen and chlorine. No contamination was found on these samples.

3.4.1.2. XPS Quantitative Analyses

The results of the quantitative analyses for UV (300 nm) photo-chlorination of MWCNT paper with Cl_2 gas is summarized in Table 8. Figure 23 depicts the atomic percent of chlorine and oxygen versus treatment time for MWCNT paper UV photo-chlorinated with Cl_2 gas.

Two control experiments (samples 5B and 9B in Table 8) were conducted with MWCNT paper treated for 60 min in the presence of Cl_2 gas and without UV radiation. The amounts of Cl detected were *ca.* 0.85 at%, and the amounts of O detected were *ca.* 1.75 at% which is within experimental error of the untreated MWCNT samples (Table 8). The average amount of oxygen for 8 untreated samples was calculated to be 1.9 ± 0.8 at% which is in good agreement with previous measurements [71] (Table 1, Table 5). The amount of chlorine on the sample's surface increased with increasing treatment time of exposure up to 30 – 90 min where a plateau value is reached at *ca.* 13 at% Cl. For the

initial *ca.* 20 min of treatment, the at% O is within experimental error of the untreated samples while at longer treatment times the amount increases to *ca.* 5 at%.

Table 8. Results of XPS quantitative analyses for UV photo-chlorination of MWCNT paper with Cl_2 gas

Sample	at% C	at% O	at% Cl
Control (untreated), average of 8 controls	98.1 ± 0.8	1.9 ± 0.8	0.0
15B, Treated, 1 min	97.8	0.8	1.4
15C, Treated, 2 min	97.2	0.8	2.1
15D, Treated, 3 min	95.6	0.8	3.7
15E, Treated, 8 min	93.2	1.3	5.6
16B, Treated, 10 min	94.0	1.0	5.1
19A, Treated, 20 min	85.3	2.8	11.9
21A, Treated, 30 min	84.6	5.7	9.7
19B, Treated, 45 min	82.9	2.0	15.1
19C, Treated, 65 min	83.5	4.0	12.5
21B, Treated, 90 min	81.0	5.4	13.0
5B, Treated, 60 min without UV radiation	97.8	1.3	0.8
9B, Treated, 60 min without UV radiation	96.7	2.2	0.9

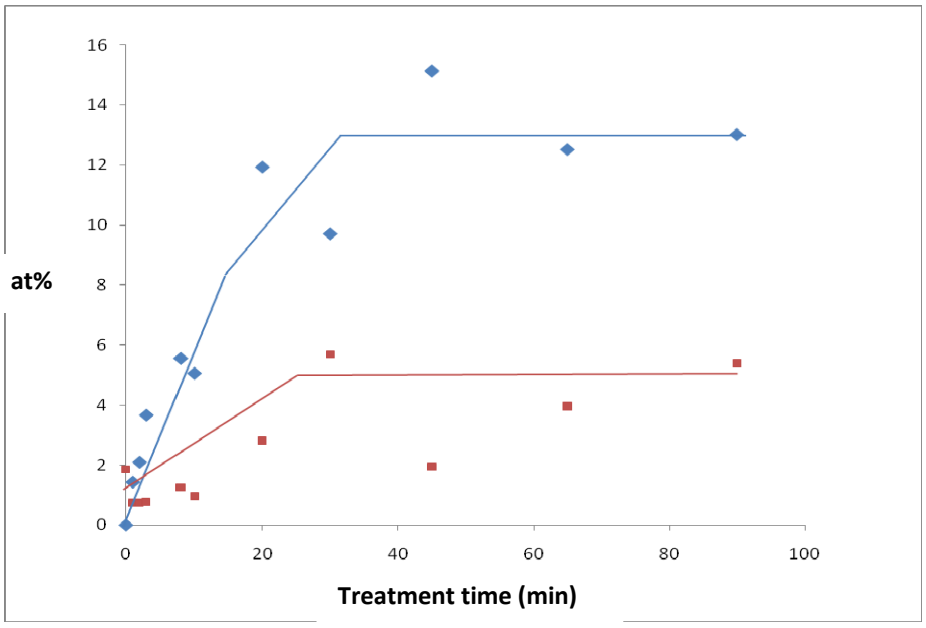

Figure 23. Plot of at% Cl (♦) and O (■) for control MWCNT paper and samples UV photo-chlorinated with Cl_2 gas as a function of exposure time.

3.4.1.3. XPS Chemical State Analyses

Figures 24, 25 and 26 show the overlapped C 1s, Cl 2p and O 1s spectra, respectively, for MWCNT paper samples treated for 20, 30, 45 and 65 min (samples 19A, 21A, 19B and 19C in Table 8, respectively) with UV photo-chlorination. The principal peak at 284.8 eV in Figure 24 dominates the spectra and it is due to sp^2-hybridized carbon bonding. At higher binding energies (286 – 288 eV) complex spectral features due to C-O and C-Cl bonding are evident. The intensities of the high binding energy peaks increased with exposure time as expected from the quantitative analyses (Table 8) which showed an increase in oxygen and chlorine concentrations with length of exposure.

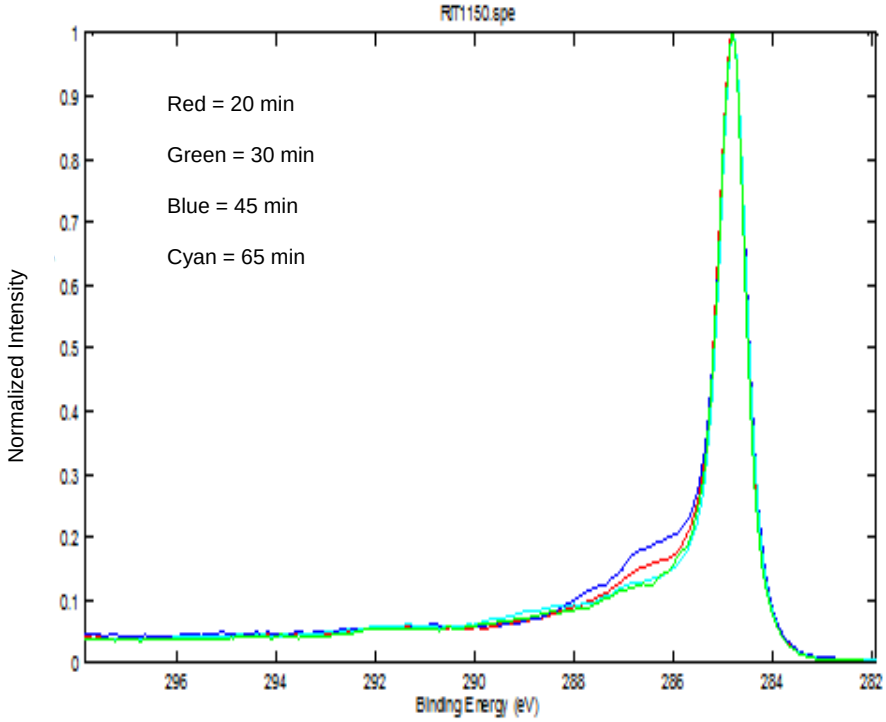

Figure 24. Overlapped C 1s XPS spectra for MWCNT paper UV photo-chlorinated for 20, 30, 45 and 65 min with Cl_2 gas.

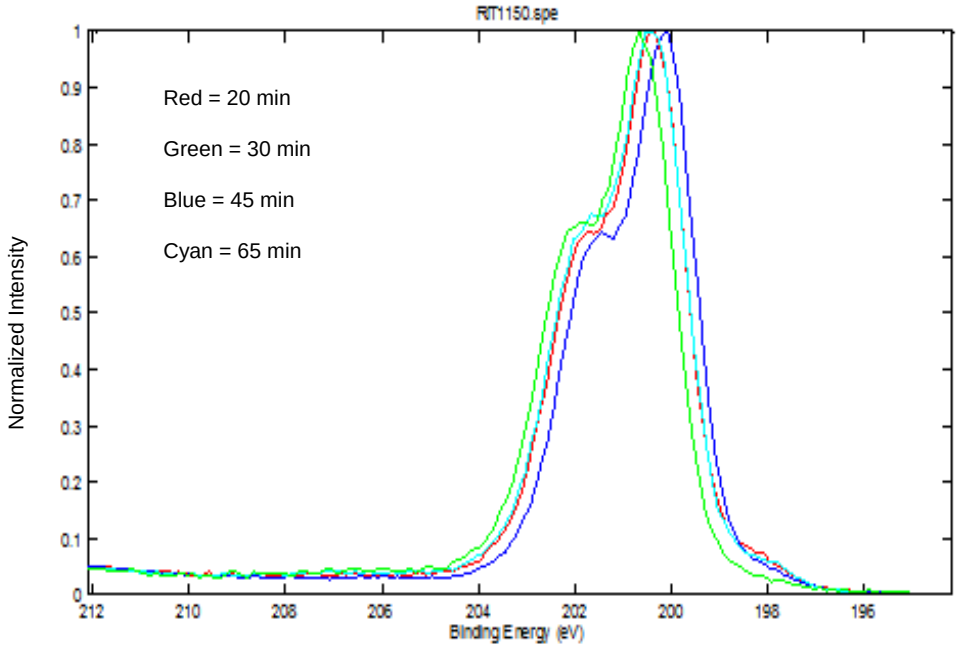

Figure 25. Overlapped Cl 2p XPS spectra for MWCNT paper UV photo-chlorinated for 20, 30, 45 and 65 min with Cl_2 gas.

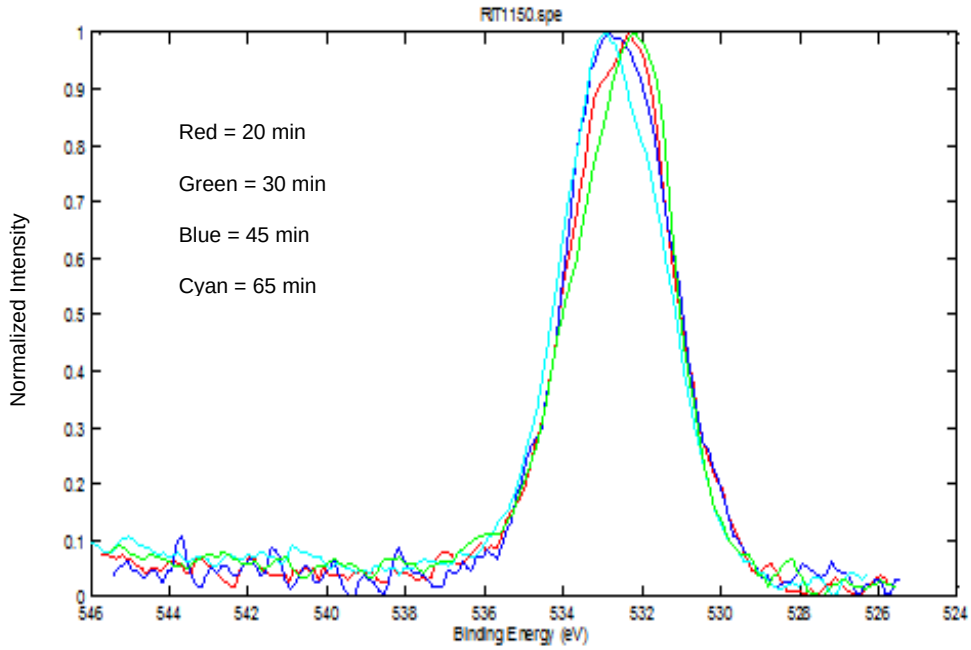

Figure 26. Overlapped O 1s XPS spectra for MWCNT paper UV photo-chlorinated for 20, 30, 45 and 65 min with Cl_2 gas.

Binding energy values reported in the literature [89] were utilized to assign the peaks reported in Table 9 with the curve fitting results of the C 1s spectrum (Figure 27) for the sample treated for 45 min (sample 19B in Table 8) which showed the highest level of chlorination with the at% O within the error limits of the untreated MWCNTs. The Cl 2p and O 1s spectra are difficult to curve fit because the two peaks that appear in the Cl 2p spectra (Figure 25) are not due to different chemical states but arise from two spin orbital components, $^2P_{3/2}$ and $^2P_{1/2}$, and the O 1s spectra (Figure 26) show a single peak without any resolvable structure.

Table 9. Results of absolute % of C-containing groups for the MWCNT paper sample UV photo-chlorinated for 45 min (19B) with Cl_2 gas

Assignment	**B. E. (eV)**	**Treated, 45 min (19B)**
C-C sp^2	284.8	49.8
C-C sp^3, -C*H=C-C*H_2 | Cl	285.6	9.3
C*-CCl_2, -CH=C*-CH_2, ether, glycol | Cl	286.2	5.1
Energy Loss	286.5	4.6
Epoxide ring C, -CH=C*H-Cl	287.2	6.5
O-C-O, Energy Loss	287.6	2.2
C-C*Cl_2, O-C=O	288.6	1.3
Energy Loss	289.3	1.7
Energy Loss	290.8	1.1
Energy Loss	292.2	1.3
		Total = 82.9

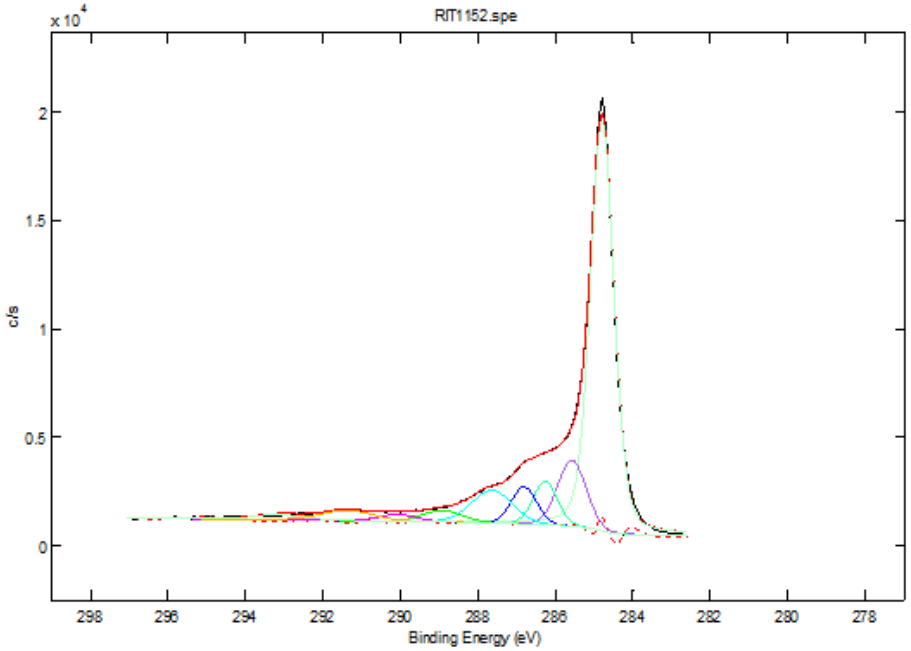

Figure 27. XPS C 1s curve fitting for MWCNT paper UV photo-chlorinated for 45 min (19B) with Cl_2 gas.

3.4.2. SWCNT powder

3.4.2.1. XPS Qualitative Analyses

The control SWCNT powder contained only carbon and oxygen. The treated samples contained carbon, oxygen, chlorine and cobalt.

3.4.2.2. XPS Quantitative Analyses

The results of the quantitative analyses for UV (300 nm) photo-chlorination of SWCNT powder with Cl_2 gas is summarized in Table 10. Carbon, oxygen, chlorine and cobalt are reported in units of atomic percent (at%).

Table 10. Results of XPS quantitative analyses for UV photo-chlorination of SWCNT powder with Cl_2 gas

Sample	at% C	at% O	at% Cl	at% Co
10A, Control (untreated)*	96.1	3.9	0.0	---
11A, Treated, 15 min	84.6	3.9	11.5	---
11B, Treated, 30 min	61.3	2.7	36.0	---
11C, Treated, 60 min	60.1	2.9	37.0	---
17A, Control (untreated)*	91.4	8.6	0.0	---
14G, Treated, 1 min	90.7	6.2	2.3	0.2
14A, Treated, 2 min	88.47	8.1	3.1	0.5
14H, Treated, 3 min	90.0	7.3	2.4	0.3
14B, Treated, 5 min	86.1	6.3	7.4	0.2
14C, Treated, 8 min	86.9	6.5	6.2	0.4
14I, Treated, 10 min	83.9	7.6	8.4	0.2
14D, Treated, 12 min	86.6	5.9	7.4	0.1
14E, Treated, 20 min	85.8	6.4	7.6	0.3
17C, Treated, 20 min*	86.3	6.9	6.4	0.2
22A, Treated, 20 min*	81.3	9.3	9.4	---
17B, Treated, 25 min*	85.9	6.9	7.0	0.2
22B, Treated, 25 min*	82.0	8.6	9.4	---
22C, Treated, 40 min	82.2	8.6	9.1	---
17E, Treated, 45 min	80.7	8.2	10.8	0.3
22D, Treated, 50 min	82.3	9.0	8.8	---
14F, Treated, 60 min without UV radiation	89.0	7.9	2.7	0.4

* Replicate samples

One control experiment (sample 14F in Table 10) was conducted with SWCNT powder in the presence of Cl_2 gas for 60 min without UV radiation. The amounts of Cl and O detected were 2.7 at% Cl and 7.9 at% O, respectively. The untreated sample with 3.9 at% O (10A) was the control of the samples treated for 15, 30 and 60 min (11A, 11B and 11C). It is observed from Table 10 that these samples (Series 11A-11C) maintained their low amounts of oxygen and achieved high saturation levels of chlorine (*ca.* 36 at%) after treatment. The untreated sample with 8.6 at% O (17A) was the control of the samples treated from 1 to 50 min (Series 14A-14I, Series 17B-17E and Series 22A-22D). It is observed that the chlorine concentration increased with increasing treatment time but due to the presence of high amounts of oxygen in the samples, the resulting saturation levels of Cl after treatment were low (max. of 10.8 at% Cl at 45 min). The detected amount of oxygen was not a function of exposure time and varied independently of treatment time.

3.4.2.3. XPS Chemical State Analyses

Wide scan spectra in the binding energy range from 0 to 1200 eV were obtained to identify the elements present on the surface a SWCNT powder sample UV photo-chlorinated for 20 (sample 17C in Table 10) and 30 min (sample 11B in Table 10). The XPS wide scan spectra are shown in Figure 28.

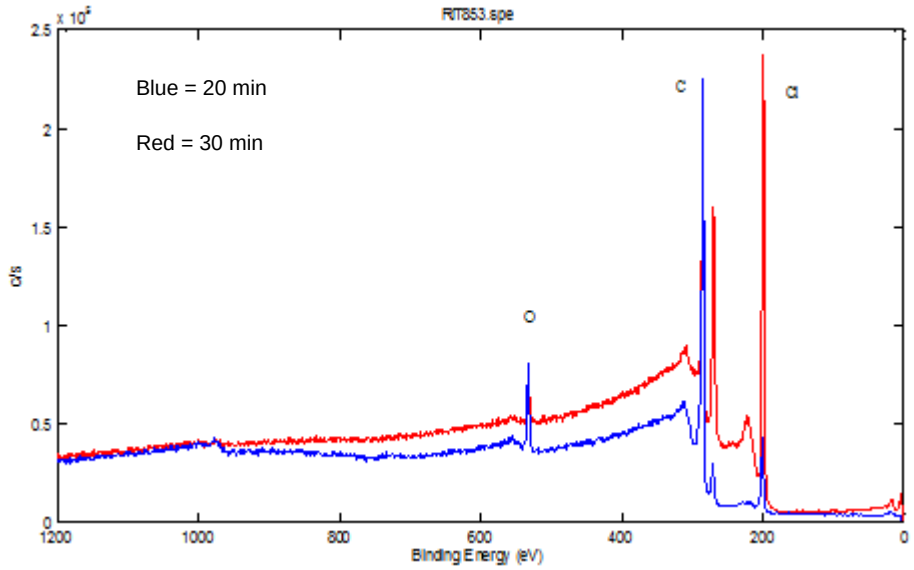

Figure 28. XPS wide scan spectra of the modified surface of SWCNT powder UV photo-chlorinated for 20 (17C) and 30 min (11B) with Cl_2 gas.

The results of the curve fitting for the C 1s peak of the sample treated for 60 min (sample 11C in Table 10) are shown in Figure 29. The intensities of the high binding energy peaks increase with exposure time as expected from the quantitative analyses (Table 10) which show an increase in oxygen and chlorine concentrations with length of exposure. The principal peak due to sp^2-hybridized carbon bonding at 284.8 eV dominates the spectrum. The tail from 286 to 290 eV is built as a complex spectral feature due to C-O and C-Cl bonding.

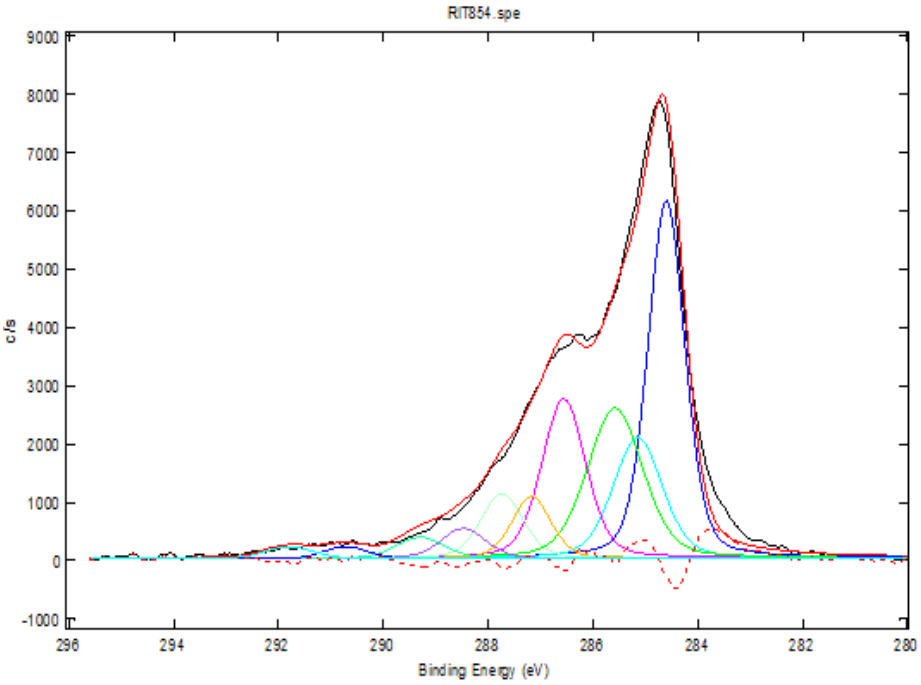

Figure 29. Results of the curve fitting for the C 1s peak of the SWCNT powder sample UV photo-chlorinated for 60 min (11C) with Cl_2 gas.

Curve fitting was completed in order to assign the peaks, binding energies and absolute-carbon percentage. The methodology used was the same as previously described in section 3.2.3. Figure 30 shows the results of the curve fitting for the C 1s spectra of the powdered control SWCNT and samples treated for 15, 30 and 60 min (Series 11A-11C in Table 10) which revealed high saturation levels of chlorine. The quantitative analysis of the control (sample 6A in Table 2) detected 95.0 at% C and 5.0 at% O.

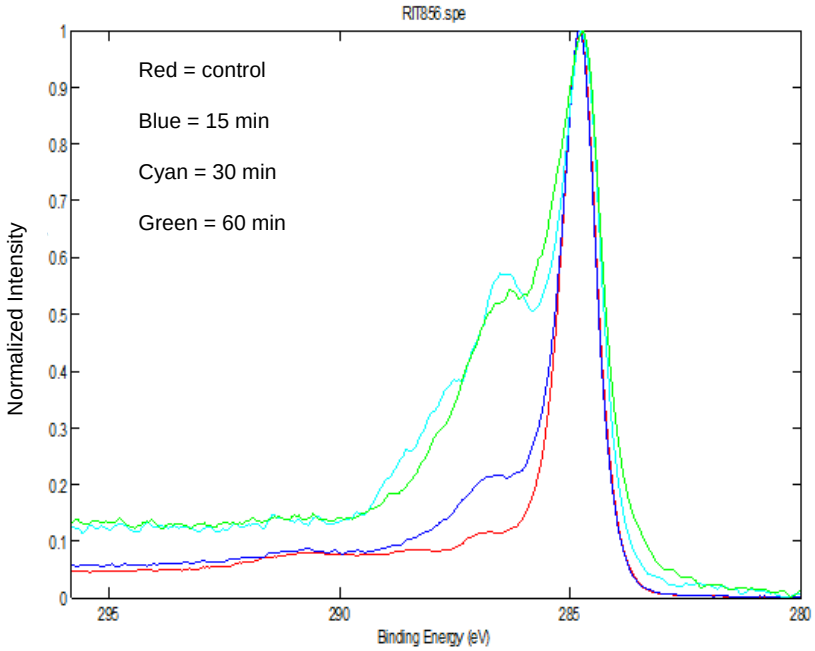

Figure 30. Overlapped C 1s spectra for control SWCNT powder and samples treated for 15, 30 and 60 min with Cl_2 gas and UV radiation.

Table 11 shows the results of the curve fitting for the C 1s peaks of the control (sample 6A) and powdered SWCNT sample treated for 60 min (11C) which presented a high saturation level of chlorination (37 at% Cl). There was a dramatic decrease of the sp^2- and sp^3-hybridized carbon as a result of the chlorine-functionalization. At the B. E. of 287.2 eV, the absolute % of carbon had a slight increase in comparison to the control due to the addition of the –CH=C*H-Cl moiety. Only a very small amount of the C-Cl_2 and/or O-C=O moieties were present and were not affected by the length of treatment or the presence of radiation. The concentration of the O-C-O moiety was also not affected by treatment time.

Table 11. Results of absolute % of C-containing groups for the control (6A) and SWCNT powder sample treated for 60 min (11C) with Cl_2 gas and UV radiation

B. E. (eV)	**Assignment**	**Control [a] (6A)**	**Assignment**	**Treated, 60 min (11C)**
284.8	C-C sp^2	46.6	C-C sp^2	18.5
285.6	C-C sp^3	22.2	C-C sp^3, -C*H=C-C*H_2 | Cl	8.4
286.2	ether, glycol	5.2	ether, glycol, C*-CCl_2, -CH=C*-CH_2, | Cl	11.6
286.5	Energy Loss	2.4	Energy Loss	9.8
287.2	Epoxide ring C	2.8	Epoxide ring C, -CH=C*H-Cl	3.4
287.6	O-C-O, Energy loss	3.6	O-C-O, Energy Loss	3.8
288.6	O-C=O	1.4	C-C*Cl_2, O-C=O	1.9
289.3	Energy Loss	4.1	Energy Loss	1.4
290.8	Energy Loss	4.6	Energy Loss	0.6
292.2	Energy Loss	2.2	Energy Loss	0.7
		Total = 95.0		Total = 60.1

[a] Quantitative analyses: 95.0 at% C and 5.0 at% O.

Table 12 summarizes the peak area % by chemical species for the control (sample 6A) and powdered SWCNT samples treated from 1 to 50 min (samples Series 14A-14I and 22A-22D in Table 10) which revealed low saturation levels of chlorine after

treatment due to the high oxygen concentration present on these samples before UV photo-chlorination.

Table 12. Summary of the C 1s curve fitting peak area % for the control and powdered SWCNT samples treated from 1 to 50 min with Cl_2 gas and UV radiation

Time (min)	at% O	at% Cl	ether, glycol, -C*H=CH-Cl, C*-CCl_2, C*R_2-CR-Cl	Epoxide ring C, CH=C*H-Cl	O-C-O	C-C*Cl_2, O-C=O
control	5.0	0.0	5.2	2.8	3.6	1.4
1	6.2	2.9	6.6	5.3	3.3	1.6
2	8.1	3.1	5.0	4.2	3.4	1.2
3	7.3	2.4	6.9	4.5	3.2	1.7
5	6.3	7.4	7.4	8.4	3.4	1.4
8	6.5	6.2	7.6	7.6	3.6	1.5
10	7.6	8.4	7.8	7.3	3.5	1.6
12	5.9	7.4	8.0	6.4	4.7	1.1
20*	6.4	7.6	6.1	5.5	4.6	1.0
20*	9.3	9.4	4.4	6.1	3.0	3.0
25	8.6	9.4	4.2	7.1	3.5	2.5
40	8.6	9.1	5.3	7.2	3.6	2.6
50	9.0	8.0	4.5	6.1	3.0	2.9

* Replicate sample

The nanotubes treated for 1, 2 and 3 minutes exhibited the lowest concentrations of chlorine on the surface while the nanotubes UV photo-chlorinated for longer treatment times exhibited higher chlorine concentrations. This appears, from the results from Table 12, to be due to the presence of greater numbers of CH=CH-Cl and CR_2-CR-Cl moieties on the samples treated longer than 3 minutes. There is very little evidence for the presence of the C-Cl_2 moiety.

Figure 31 shows the absorption spectrum of Cl_2 [75], for which absorption maximum is at 330 nm.

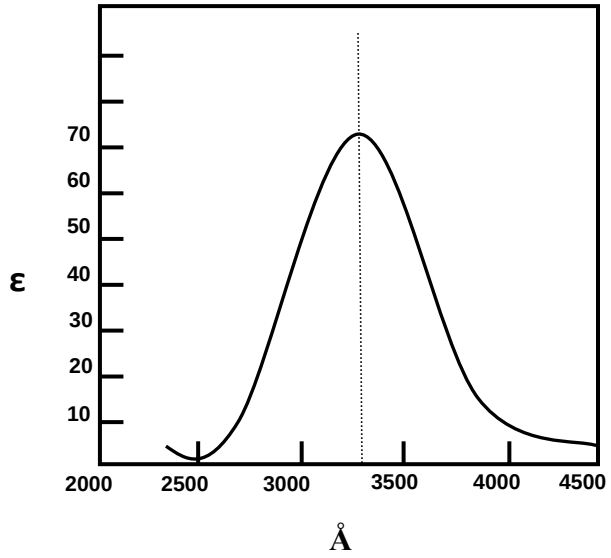

Figure 31. Absorption spectrum of $Cl_2(g)$ (ε is in units of liters/mole-cm) [75].

The transition responsible for this band is assumed to be a singlet-triplet promotion symbolized by (6) [75]:

$$Cl_2(^1\sum_g^+) + h\nu \rightarrow Cl_2(^3\Pi_u) \qquad (6)$$

The absorption of a quantum of light by a chlorine molecule, over most of the spectral range absorbed by Cl_2 (Figure 31), results for the most part in the formation of chlorine atoms [75]. If the absorption occurs in the continuum of the spectrum, dissociation occurs from the original state of the excited molecule and, one normal ($^2P_{3/2}$) and one excited ($^2P_{1/2}$) halogen atom may be formed (equation 6a) [75].

$$Cl_2(^1\sum_g^+) + h\nu \rightarrow Cl_2(^3\Pi_0^+{}_u) \rightarrow Cl(^2P_{3/2}) + Cl(^2P_{1/2}) \qquad (6a)$$

If the absorption occurs at wavelengths that are of sufficient energy to break the bond (ΔE^o_{298} = 498.9 nm, for $Cl_2(g) \rightarrow 2Cl(g)$), in this case, two ground-state ($^2P_{3/2}$) atoms are formed (equation 6b) [75].

$$Cl_2(^1\sum_g^+) + h\nu \rightarrow Cl_2(^3\Pi_0^+{}_u)$$
$$\downarrow (+M)$$
$$Cl_2(^3\Pi_{1u}) \rightarrow 2\ Cl(^2P_{3/2}) \qquad (6b)$$

SWCNTs [52] and MWCNTs [66] were functionalized at room temperature and atmospheric pressure by ball milling in a reactive atmosphere of gaseous Cl_2. This method was shown to be effective for the production of functionalized nanotubes with up to 5.1 wt% Cl for SWCNTs [52]. Our current UV (*ca.* 300 nm) photochemical procedure may be applicable for nanoelectronic devices where control is needed of the metallic and semiconducting properties of the functionalized CNTs. The saturation levels of 0.85 at% Cl for MWCNT paper (Table 8) and 2.7 at% Cl for SWCNT powder (Table 10) treated for 60 min with gaseous Cl_2 in the absence of photons was shown to be slow relative to photo-chlorination where Cl atoms, that are photo-chemically produced [75], readily add across the π-conjugated system [53] in the carbon nanotube structure. The

chlorine-containing radical may react either with Cl_2 to form a dichloro-moiety or O_2 to generate ultimately chlorine-containing oxygenated products [76].

Figure 23 shows a steady increase in the Cl and O concentrations on the surface of MWCNT paper with treatment time up to a saturation level of *ca.* 13 at% Cl and *ca.* 5 at% O. The oxygen concentrations detected for MWCNT paper (Table 8, Figure 23) might be from impurities, vacuum line leakage or due to reaction of radicals on the surface of the CNTs with oxygen in air when the sample is removed from the photochemical cell. The binding energies of Cl $2p_{3/2}$ and Cl $2p_{1/2}$ at 200.5 and 202.1 eV, respectively, in Figure 25, indicate that chlorine atoms were covalently bonded to sp^2 carbon [52, 94].

Table 10 shows an increase in the Cl concentration of SWCNT powder samples with time of exposure to Cl_2 and UV radiation. The first SWCNT control (sample 10A) revealed low amounts of oxygen (3.9 at% O). Sample 11C showed a maximum of 37 at% Cl and 2.9 at% O after 60 min of treatment. On the other hand, a high oxygen concentration of 8.9 at% O in the second SWCNT control (sample 17A) resulted in lower saturation levels of chlorine on the surface of SWCNT powder after treatment with Cl_2 and UV radiation. The maximum saturation level of chlorine was obtained for the sample treated for 45 min (17E) which revealed 10.8 at% Cl and 8.2 at% O. The available active sites for introduction of chlorine onto the SWCNT's surface were occupied by high amounts of oxygen making it difficult for Cl atoms to replace O and thus, resulted in a low Cl concentration on the sample's surface after treatment. The availability of active sites on samples 11A, 11B and 11C due to low concentrations of

oxygen resulted in high saturation levels of chlorine on the surface after treatment with Cl_2 and UV radiation.

The wide scan XPS spectra in Figure 28 show distinct oxygen, carbon and chlorine peaks representing the major constituents of the SWCNT powder's surface. The binding energies associated with O, C and Cl peaks in Figure 28 are in good agreement with those reported by Lee et al. [55]. Tables 9 and 11 show the oxygenated and chlorinated species that account for the observed C 1s XPS spectra (Figures 27 and 29) of MWCNT paper and SWCNT powder, respectively, after UV photo-chlorination with Cl_2 gas. The XPS curve fitting has assigned four peaks for C-Cl species at 285.6, 286.2, 287.2 and 288.6 eV while Lee et al. [55] reported only one C-Cl species peak assigned at 287.7 eV [52, 55]. The peak at *ca.* 291 eV in Figures 27 and 29 is characteristic of the shake-up of the sp^2-hybridized carbon atoms [52, 66].

3.5. UV photo-chlorination of SWCNT powder with HCl gas

3.5.1. XPS Qualitative Analyses

The control SWCNT powder contained only carbon and oxygen. The treated samples contained carbon, oxygen and chlorine. The samples treated for 5, 10, 20, 30, 45, 60 and 90 min presented also cobalt.

3.5.2. XPS Quantitative Analyses

The results of the quantitative analyses for UV (184.9 and 253.7 nm) photo-chlorination of SWCNT powder with HCl is summarized in Table 13. Figure 32 depicts the atomic percent of chlorine and oxygen versus treatment time in minutes for SWCNT powder UV photo-chlorinated with HCl gas. The control sample (24A in Table 13) contained a higher amount of oxygen (6.9 at% O) compared with previous measurements (4.9 at% O [20] and 4.7 at% O in Table 2). The oxygen concentration on the sample's surface is not a function of exposure time and showed to be higher than the Cl which resulted in lower saturation levels of chlorination after treatment with HCl and UV radiation. Table 13 and Figure 32 present a steady increase in the Cl concentration up to a saturation level of *ca.* 5.75 at% Cl at treatment times of 60 – 90 min. Analyses of the samples showed that some of them contained small amounts of cobalt after treatment.

Table 13. Results of XPS quantitative analyses for UV photo-chlorination of SWCNT powder with HCl gas

Sample	at% C	at% O	at% Cl	at% Co
24A, Control (untreated)	93.0	6.9	0.0	---
24B, Treated, 1 min	92.6	6.5	0.9	---
24C, Treated, 2 min	92.2	6.6	1.3	---
24D, Treated, 3 min	90.0	8.0	1.9	---
24E, Treated, 5 min	92.4	5.0	2.0	0.5
24G, Treated, 10 min	89.9	7.4	2.6	0.1
24I, Treated, 20 min	91.7	5.5	2.2	0.6
24J, Treated, 30 min	89.0	7.4	3.4	0.2
24K, Treated, 45 min	80.4	14.0	5.1	0.5
24L, Treated, 60 min	86.3	7.8	5.8	0.2
24M, Treated, 90 min	84.6	9.5	5.7	0.2

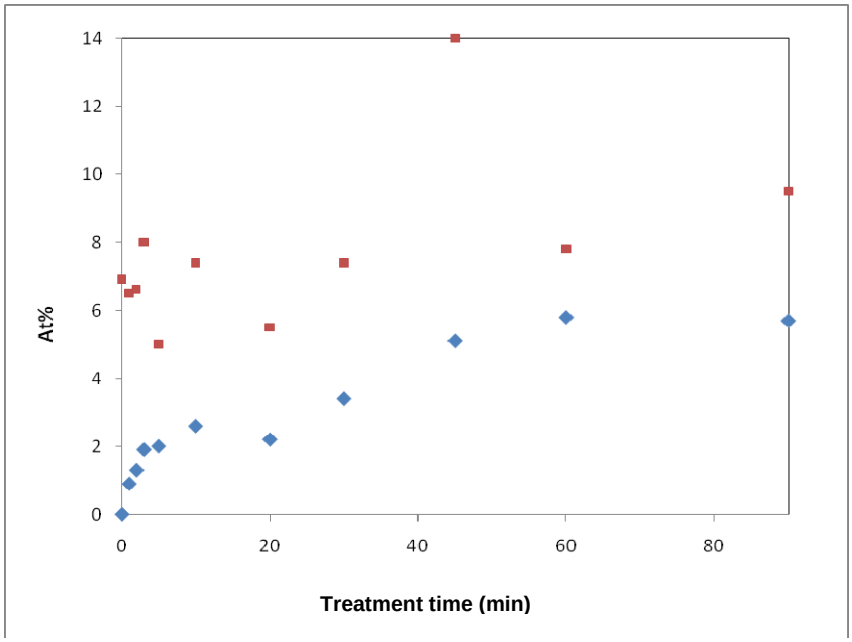

Figure 32. Plot of at% Cl (♦) and O (■) for control SWCNT powder and samples UV photo-chlorinated with HCl gas as a function of exposure time.

3.5.3. XPS Chemical State Analyses

The results of the curve fitting for the C 1s peak of the powdered SWCNT control (sample 24A in Table 13) are shown in Figure 33. Figure 34 shows the results of the overlapped XPS C 1s spectra of the powdered SWCNT samples treated for 20, 30, 45, 60 and 90 min (samples 24I-24M in Table 13) with gaseous HCl and UV radiation. The intensities of the binding energy peaks increase with exposure time as expected from the quantitative analyses (Table 13) which show an increase in chlorine concentration with length of exposure. The principal peak due to sp^2 C-C bonding at 284.8 eV dominates the spectra. The tail from 286 to 290 eV is built as a complex spectral feature due to C-O and C-Cl bonding.

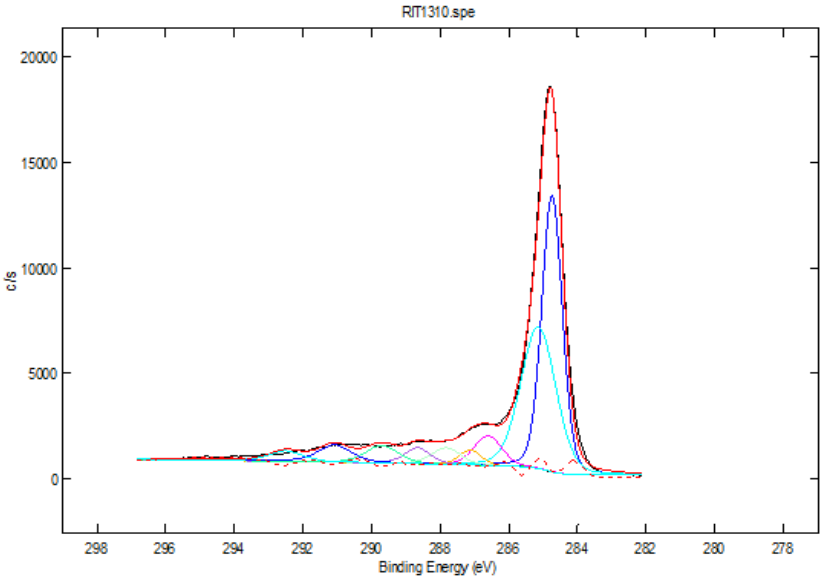

Figure 33. Results of the curve fitting for the C 1s spectrum obtained for the control (SWCNT powder sample.

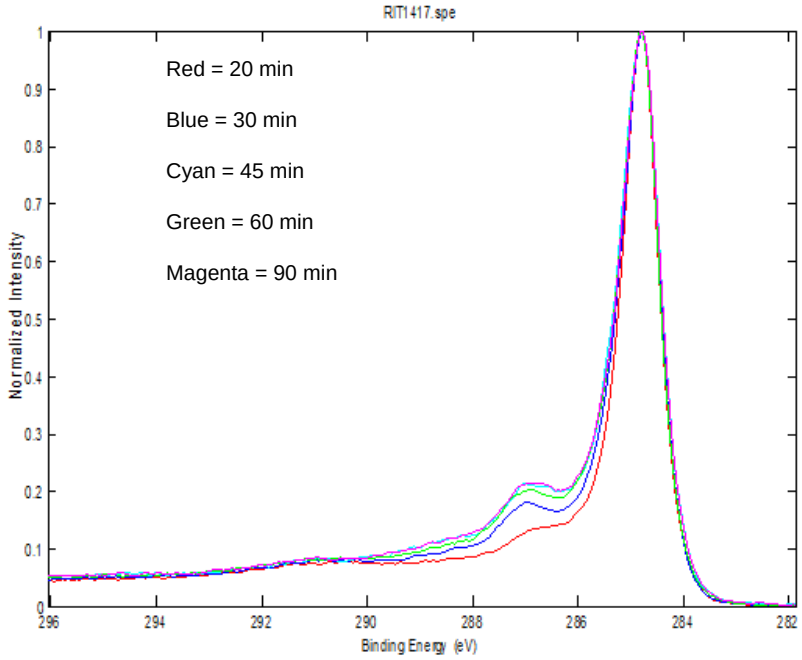

Figure 34. Overlapped C 1s spectra for SWCNT powder samples treated for 20, 30, 45, 60 and 90 min with HCl gas and UV radiation.

Curve fitting was completed in order to assign the peaks, binding energies and absolute-carbon percentage. The methodology used was the same as previously described in section 3.2.3. Table 14 shows the results of the curve fitting for the C 1s peaks of the control (24A) and SWCNT powder treated for 60 min (24L) with gaseous HCl and UV radiation which presented the highest saturation level of chlorine (5.8 at%).

Table 14. Results of absolute % of C-containing groups for the control (24A) and SWCNT powder sample UV photo-chlorinated for 60 min (24L) with HCl

B. E. (eV)	**Assignment**	**Control (24A)**	**Assignment**	**Treated, 60 min (24L)**
284.7	C-C sp^2	36.7	C-C sp^2	34.6
285.2	C-C sp^3	32.3	C-C sp^3	29.6
285.9	ether, glycol	3.2	ether, glycol -C*H=CH-Cl, C*-CCl_2, C*R_2-CR-Cl |	3.5
286.6	Energy Loss	2.3	Energy Loss	1.9
287.1	Epoxide ring C	2.0	Epoxide ring C, -CH=C*H-Cl	6.6
287.9	O-C-O, Energy loss	3.2	O-C-O, Energy loss	1.5
288.6	O-C=O	0.3	C-C*Cl_2, O-C=O	1.5
289.5	Energy Loss	3.8	Energy Loss	2.2
290.9	Energy Loss	4.2	Energy Loss	2.2
292.3	Energy Loss	2.5	Energy Loss	2.7
		Total = 93.0		Total = 86.3

The data shows a slight decrease of the sp^2- and sp^3-hybridized carbon as a result of the chlorine-functionalization. At the binding energy of 287.1 eV, the absolute % of carbon of the sample treated for 60 min shows an increase compared to the control due to the appearance of the –CH=C*H-Cl moiety. The concentration of the O-C-O moiety at 287.9 eV suffered a decrease relative to the control. At the B.E. of 288.6 eV, the absolute-C % of the 60 min treated sample shows an increase in comparison to the control due to the addition of the C-C*Cl_2 functional group onto the SWCNT powder's surface.

Table 15 summarizes the peak area % by chemical species for the control (24A) and powdered SWCNT samples treated from 1 to 90 min (24B-24M in Table 13) which revealed low saturation levels of Cl after treatment due to the high oxygen concentration present on these samples before UV photo-chlorination with HCl gas. There is a steady increase in the Cl concentration up to a saturation level of *ca.* 5.8 at%. The amount of detected oxygen increased with treatment time but not in a linear or proportional relationship. The concentration of oxygen is higher than that of chlorine and thus, resulted in low saturation levels of Cl onto the sample's surface. The data shows that only a very small amount of the C-C*Cl_2 and/or O-C=O moieties are present and are not affected by the length of treatment time or the presence of radiation. The concentration of the O-C-O moiety is also not a function of treatment time or conditions. The nanotubes treated for 45, 60 and 90 min exhibited the highest concentrations of chlorine on the surface due to the presence of greater numbers of CH=CH-Cl and CR_2-CR-Cl moieties on these samples.

Table 15. Summary of the C 1s curve fitting peak area % for the control and powdered SWCNT samples treated from 1 to 90 min with HCl gas and UV radiation

Time (min)	at% O	at% Cl	Ether, glycol, -C*H=CH-Cl, C*-CCl_2, C*R_2-CR-Cl	Epoxide ring C, CH=C*H-Cl	O-C-O	C-C*Cl_2, O-C=O
control	6.9	0.0	3.2	2.0	3.2	0.3
1	6.5	0.9	1.9	5.1	2.2	2.7
2	6.6	1.3	2.0	5.2	2.1	2.6
3	8.0	1.9	1.9	5.8	2.3	2.3
5	5.0	2.0	2.2	4.8	2.8	2.0
10	7.4	2.6	2.9	5.7	2.5	2.0
20	5.5	2.2	2.0	7.4	2.8	2.6
30	7.4	3.4	3.2	8.6	3.9	2.6
45	14.0	5.1	4.3	9.2	2.0	2.0
60	7.8	5.8	3.5	6.6	1.5	1.5
90	9.5	5.7	3.5	7.6	1.5	1.5

The ground state of hydrogen chloride is $X^1\sum^+$, D_0(H-Cl) = 4.431 ± 0.002 eV [79]. The absorption coefficients of the continuous region from 138.0 to 200.0 nm are given in Figure 35 [79].

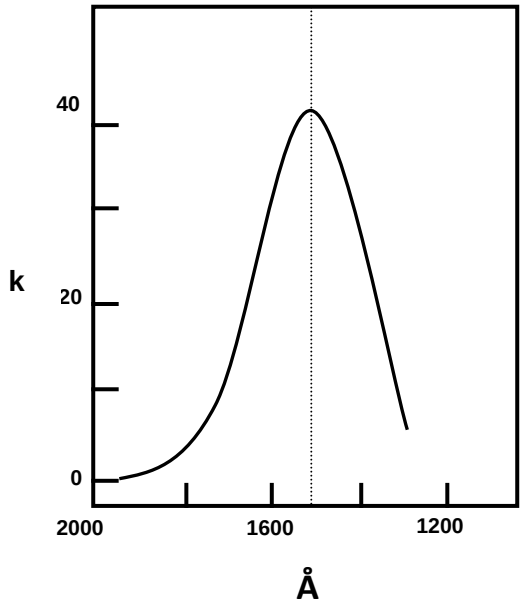

Figure 35. Absorption spectrum of HCl (k is in units of $atm^{-1}cm^{-1}$, base 10 at room temperature) [79].

Hot H atoms having kinetic energy of about 2.27 eV are produced by photolysis at 184.9 nm [79]. Production of H + Cl is most likely the primary process. The Cl atoms are in the ground $^2P_{3/2}$ state. The following photochemical reactions (7), (8) and (9) are the ones expected [79]:

$$HCl + h\nu \rightarrow H + Cl(^2P_{3/2}) \qquad (7)$$

$$H + HCl \rightarrow H_2 + Cl \qquad (8)$$

$$Cl + Cl + M \rightarrow Cl_2 + M \qquad (9)$$

Previously, SWCNT samples [53] were functionalized by means of a hydrothermal treatment (HT) in an aqueous acidic solution of 5M HCl inserted into a sealed autoclave under vacuum filled with CO_2 and heated up to 250 or 500 ^oC with treatment times of 24 or 114 hours. HT of SWCNTs showed to be an efficient method for attaching chlorine to the conjugated π-system of the material, however, the achieved saturation level of chlorine was very low (*ca.* 0.4 at% Cl) [53]. Their reported oxygen concentration for the pristine SWCNTs was 6 at% O and after hydrothermal treatment with an acidic solution of 5M HCl, saturation levels of oxygen were reported to range from 9 to 17 at% O. Chlorine atoms were introduced at structurally/electronically disordered defect sites as suggested by XPS and UV photoemission spectroscopy [53].

Table 13 shows that UV (184.9 and 253.7 nm) photo-chlorination of SWCNT powder with HCl with gas was a very efficient technique to functionalize the sample's surface with chlorine atoms up to a saturation level of *ca.* 5.8 at% Cl. Our control sample (24A in Table 13) presented 6.9 at% O. The detected amount of oxygen in this experiment was higher than our previous measurements ([20], Table 2). After UV photolysis with HCl gas, SWCNTs presented amounts of oxygen ranging from 5.0 to 14.0 at% O (Table 13).

According to the analyses of the XPS C 1s spectra of the samples (Figures 33 and 34) and curve fittings (Tables 14 and 15), an increased fraction of the carbon sites on the surface were oxidized as well as chlorinated groups were created. UV photo-chlorination of SWCNT powder with HCl gas (Tables 14 and 15) showed similar functional groups from MWCNT paper (Table 9) and SWCNT powder (Tables 11 and 12) UV photo-chlorinated with Cl_2 gas. The Cl was reported to be bound to conjugated

π-systems in polymers [53] which is correspondent to the resulting C-Cl binding energy of approximately 200 eV in the XPS Cl 2p spectra (Figure 25).

The oxygen concentration detected on the surface of SWCNT powder UV photo-chlorinated with HCl gas was higher than the concentration of chlorine atoms detected. As with UV photolysis of Cl_2 gas in the presence of SWCNT powder, the active sites available for Cl functionalization were occupied and mostly saturated with oxygen and thus, resulted in low saturation levels of chlorine on the surface of the samples. The increased amount of oxygen observed with increasing treatment time might be due to vacuum line leakage, presence of impurities, or due to the reaction of radicals on the sample's surface with oxygen in air when the sample is removed from the photochemical cell.

4. Conclusions

Dry, gas-phase surface modification of carbon nanotubes with oxygen in the presence and absence of radiation, and chlorination in the presence of UV radiation showed to be an effective method to add oxygenated and chlorinated functional groups to the surface of CNTs as well as eliminate the liquid waste generated originally from liquid precursors.

UV photo-oxidation of MWCNT paper yielded a saturation level of 2.8 ± 0.4 at% O at 95% confidence limits which was substantially lower than that observed via VUV photo-oxidation (*ca.* 7.4 at% O) [71]. Previous UV photo-oxidation studies showed that SWCNT powder [20] oxidized in a similar fashion than SWCNT paper [69]. SWCNT samples photo-oxidized much more rapidly and to higher levels of oxidation than MWCNT paper, potentially due to the greater curvature (*i.e.*, strain) of the smaller single tubes' diameter than the outer shells of multi-walled tubes. Larger reactivity was observed for powdered form of CNTs than for paper form possibly due to the increased surface area of the powder. The following oxygenated functional groups: C–O–C as ether and/or epoxy, C=O, O–C=O, O=C-O-C=O and/or O-(C=O)-O were generated on the surface of the MWCNT paper after UV photo-oxidation.

SWCNT powder was surface oxidized by O atoms produced by: (1) photo-oxidation in the presence of VUV radiation (λ = 104.8 and 106.7 nm) and (2) MW plasma discharge of an Ar-O_2 mixture in the absence of radiation from the discharge. The MW discharge experiments achieved lower saturation levels of oxidation (*ca.* 16.4 at% O) than with VUV photo-oxidation (*ca.* 24 at% O). MWCNT paper

surface oxidized by O atoms produced from the MW discharge method achieved lower levels of oxidation (*ca.* 6.3 at% O) than SWCNT powder samples. This level of oxidation was also lower than the levels achieved by VUV photo-oxidation of MWCNT paper conducted in the presence of radiation (7.4 at% O) [71]. VUV-produced oxygen atoms appeared to be more reactive with MWCNT paper [71] than UV-generated ozone [20]. The ester moiety, O-C=O, formed during the VUV photo-oxidation studies of SWCNT powder and MWCNT paper [71] and MW discharge experiments of MWCNT paper may result from the reaction of O and O_2 with the sample to produce the Criegee intermediate (Figure 12 [76]). Reaction of O atoms with the sp^2-hybridized carbon bond (Figure 16 [82]) possibly results in the formation of the C-O-C (as ether and or/epoxy) moiety. The reaction of oxygen atoms (produced from the MW discharge of an Ar-O_2 mixture) with SWCNT powder revealed more of the carbonyl moiety (C=O) than the ether/epoxy functional groups [77].

Chlorine atoms produced by UV photolysis of gaseous Cl_2 readily reacted with the π-conjugation system of the nanotubes to yield saturation levels of *ca.* 37 at% Cl for SWCNT powder and 13 at% Cl for MWCNT paper. The resulting Cl 2p XPS spectra indicated that chlorine atoms were covalently bonded to sp^2-hybridized carbon. SWCNT powder samples with concentrations of oxygen lower than 3.9 at% O presented high saturation levels of chlorine (max. of 37.0 at% Cl at 60 min) while samples with higher concentrations of oxygen, ranging from 5.9 to 9.3 at% O, presented lower saturation levels of Cl (max. of 10.8 at% Cl at 45 min) after UV photo-chlorination with Cl_2 gas. The available active sites for introduction of chlorine onto the SWCNT's surface were

occupied by high amounts of oxygen making it difficult for Cl atoms to replace O and thus, resulted in a low at% Cl onto the sample's surface after treatment.

UV photolysis of gaseous HCl in the presence of SWCNT powder resulted in saturation levels of chlorine of *ca.* 5.8 at% Cl. The curve fitting results showed that the oxygenated and chlorinated functional groups obtained in this method were similar to those obtained by UV photolysis of gaseous Cl_2 in the presence of MWCNT paper and SWCNT powder. High amounts of oxygen on the surface of the samples resulted in low concentrations of chlorine after treatment due to the saturation of the active sites which were occupied by oxygen atoms impeding this way their replacement by Cl atoms. UV photo-chlorination using gaseous Cl_2 and HCl showed to be an efficient technique to add chlorinated functional groups onto the surface of carbon nanotubes. XPS results revealed that Cl atoms were added to the π-conjugation system being covalently bonded to sp^2- and sp^3-hybridized carbons of the CNT's structure.

5. Summary of accomplished and future work

Table 16 below summarizes the results of all oxidation and chlorination studies that have been done so far, and also includes the future work intended to be accomplished by Dr. G. A. Takacs' research group in the Department of Chemistry at the Rochester Institute of Technology using paper and powdered forms of SWCNTs and MWCNTs.

Table 16. Summary of results for oxidation and chlorination studies of SWCNTs and MWCNTs accomplished by Dr. G. A. Takacs' research group in the Department of Chemistry at the Rochester Institute of Technology

Functionalization study	**MWCNT powder**	**MWCNT paper**	**SWCNT powder**	**SWCNT paper**
UV photo-oxidation	Max. 7.5 at% O at 120 min [70]	2.8 ± 0.4 at% O at 60-240 min [20]	Max. 23.5 at% O at 60 min [20]	Max. 25.5 at% O at 120 min [69]
VUV photo-oxidation	Max. 9.5 at% O at 120 min [70]	*ca.* 7.4 at% O at 120-240 min [71]	*ca.* 24 at% O at 60-90 min [77]	Max. 15.8 at% O at 150 min [69]
MW discharge of O atoms	TBA	*ca.* 6.3 at% O at 60-90 min	*ca.* 16.4 at% O at 60-120 min [77]	In Progress
UV photo-chlorination with gaseous Cl_2	TBA	*ca.* 13 at% Cl at 65-90 min	Max. 37.0 at% Cl at 60 min	TBA
UV photo-chlorination with gaseous HCl	TBA	In Progress	*ca.* 5.8 at% Cl at 60-90 min	TBA

(Boxes in blue represent my work reported in this Thesis)

(TBA – to be accomplished – represents the work intended to be done)

Aside from the work presented in Table 16, the following functionalization studies are also suggested:

a) Oxidation of paper and powdered forms of SWCNTs and MWCNTs with ozone (O_3) in the absence of radiation.
b) UV photo-chlorination of carbon nanotube samples containing low levels of oxygen with gaseous HCl and Cl_2.
c) UV photo-bromination of paper and powdered forms of SWCNTs and MWCNTs with gaseous HBr.
d) Sputtering of copper onto pre-oxygenated and chlorinated carbon nanotube samples.
e) Oxidation and chlorination studies of carbon nanotube samples with different diameters of tubes.

6. References

1. S. Iijima, *Nature* **354**, 56-58 (1991).
2. V. N. Popov, *Materials Science and Engineering* **R43**, 61-102 (2004).
3. S. Iijima, T. Ichihashi, *Nature* **363**, 603-605 (1993).
4. R. Chandrasekharan, T. Walker, I. Smid, The Pennsylvania State University, College of Engineering Research Symposium, CERS 2006.
5. K. Deshmukh, K. S. V. Santhanam, *Journal of Power Sources* **159**, 1084-1088 (2006).
6. R. P. Raffaelle, B. J. Landi, J. D. Harris, S. G. Bailey, A. F. Hepp, *Materials Science and Engineering* **B116**, 233-243 (2005).
7. G. Che, B. B. Lakshmi, C. R. Martin, E. R. Fischer, *Langmuir* **15**, 750-758 (1999).
8. J. J. Gooding, *Electrochimica Acta* **50**, 3049-3060 (2005).
9. K. S. V. Santhanam, R. Sangoi, L. Fuller, *Sensors and Actuators* **B106**, 766-771 (2005).
10. J. Kong, M. G. Chapline, H. Dai, *Advanced Materials* **13**, 1384-1386 (2001).
11. G. L. Hwang, K. C. Hwang, Y. T. Shieh, S. J. Lin, *Chem. Mater.* **15**, 1353-1357 (2003).
12. B. J. Landi, C. M. Evans, J. J. Worman, S. L. Castro, S. G. Bailey, R. P. Raffaelle, *Materials Letters* **60**, 29-30 (2006).
13. Z. Jin, X. Sun, G. Xu, S. H. Goh, W. Ji, *Chemical Physics Letters* **318**, 505-510, 2000.
14. B. C. Satishkumar, E. M. Vogl, A. Govindaraj, C. N. R. Rao, *J. Phys. D: Appl. Phys.* **29**, 3173-3176 (1996).
15. B. Xue, P. Chen, Q. Hong, J. Lin, K. L. Tan, *Journal of Materials Chemistry* **11**, 2378-2381 (2001).
16. Z. Sun, X. Zhang, B. Han, Y. Wu, G. An, Z. Liu, S. Miao, Z. Miao, *Carbon* **45**, 2589-2596 (2007).
17. Y. Zhang, N. W. Franklin, R. J. Chen, H. Dai, *Chemical Physics Letters* **331**, 35-41 (2000).
18. R. Blake, Y. K. Gun'ko, J. Coleman, M. Cadek, A. Fonseca, J. B. Nagy, W. J. Blau, *Journal of the American Chemical Society* **126**, 10226-10227 (2004).
19. M. Najam-ul-Haq, M. Reiner, T. Schwarzenauer, C. W. Huck, G. K. Bonn, *Analytica Chimica Acta* **561**, 32-39 (2006).
20. M. Krysak, A. Jayasekar, B. Parekh, L. Oliveira, T. Debbies, K. S. V. Santhanam, R. A. DiLeo, B. J. Landi, R. P. Raffaelle, G. A. Takacs in: *Polymer Surface Modification: Relevance to Adhesion*, K. L. Mittal (Ed.), Vol. 5, pp. 125-137, VSP/Brill, Leiden (2009).
21. K. Deshmukh, K. S. V. Santhanam, *J. Power Sources* **159**, 1084-1088 (2006).
22. J-Y. Kwon, H-D. Kim, *J. Appl. Polym. Sci.* **96**, 595-604 (2005).
23. S. Ravindran, S. Chaudhary, B. Colburn, M. Ozkan, C. S. Ozhan, *Nano Letters* **3**, 447-453 (2003).
24. B. J. Landi, S. L. Castro, H. J. Ruf, C. M. Evans, S. G. Bailey, R. P. Raffaelle, *Sol. Energy Mater. Solar Cells* **87**, 733-746 (2005).

25. M. Croston, J. Langston, G. Takacs, T. C. Morrill, M. Miri, K. S. V. Santhanam, P. Ajayan, *Intl. J. Nanoscience* **1**, 285-293 (2002).
26. R. F. Khairoutdinov, L. V. Doubova, R. C. Haddon, L. Saraf, *J. Phys. Chem.* **B108**, 11976-11981 (2004).
27. A. Jung, R. Graupner, L. Ley, A. Hirsch, *Phys. Stat. Sol.* **B243**, 3217-3220 (2006).
28. W. Li, C. Liang, J. Qiu, W. Zhou, H. Han, Z. Wei, G. Sun, Q. Xin, *Carbon* **40**, 791-794 (2002).
29. Y. Zhang, J. Li, Y. Shen, M. Wang, J. Li, *J. Phys. Chem.* **B108**, 15343-15346 (2004).
30. S. Banerjee, S. S. Wong, *J. Am. Chem. Soc.* **125**, 10342-10350 (2003).
31. Y-X. Liu, Z-J. Du, Y. Li, C. Zhang, H-Q. Li, *Chinese J. Chem.* **24**, 563-568 (2006).
32. A. Eitan, K. Jiang, D. Dukes, R. Andrews, L. S. Schadler, *Chem. Mater.* **15**, 3198-3201 (2003).
33. Y. Qin, J. Shi, W. Wu, X. Li, Z-H. Guo, D. Zhu, *J. Phys. Chem.* **B107**, 12899-12901 (2003).
34. N. Zhang, J. Xie, V. Varadan, *Smart Mater. Struct.* **11**, 962-965 (2002).
35. M. Yudasaka, M. Zhang, S. Iijima, *Chem. Phys. Lett.* **374**, 132-136 (2003).
36. Y. Peng, H. Liu, *Ind. Eng. Chem. Res.* **45**, 6483-6488 (2006).
37. S. Banerjee, S. S. Wong, *J. Phys Chem.* **B106**, 12144-12151 (2002).
38. S. Banerjee, S. S. Wong, *Nano Letters* **4**, 1445-1450 (2004).
39. H. Hiura, T. W. Ebbesen, K. Tanigaki, *Adv. Mater.* **7**, 275-276 (1995).
40. Y. Xing, L. Liang, C. C. Chusuei, R. V. Hull, *Langmuir* **21**, 4185-4190 (2005).
41. C. Li, D. Wang, T. Liang, X. Wang, J. Wu, X. Hu, J. Liang, *Powder Technology* **142**, 175-179 (2004).
42. T. W. Ebbesen, P. M. Ajayan, H. Hiura, K. Tanigaki, *Nature* **367**, 519 (1994).
43. M. R. Smith, S. W. Hedges, R. LaCount, D. Kern, N. Shah, G. P. Huffman, B. Bockrath, *Carbon* **41**, 1221-1230 (2003).
44. H. Bubert, S. Haiber, W. Brandl, G. Marginean, M. Heintze, V. Bruser, *Diamond Related Mater.* **12**, 811-815 (2003).
45. T. I. T. Okpalugo, P. Papakonstantinou, H. Murphy, J. Mclaughlin, N. M. D. Brown, *Carbon* **43**, 2951-2959 (2005).
46. X. Lu, L. Zhang, X. Xu, N. Wang, Q. Zhang, *J. Phys. Chem.* **B106**, 2136-2139 (2002).
47. O. Byl, J. Liu, J. T. Yates, Jr., *Langmuir* **21**, 4200-4204 (2005).
48. D. B. Mawhinney, V. Naumenko, A. Kuznetsova, J. T. Yates, Jr., J. Liu, R. E. Smalley, *Chem. Phys. Lett.* **324**, 213-216 (2000).
49. D. B. Mawhinney, V. Naumenko, A. Kuznetsova, J. T. Yates, Jr., J. Liu, R. E. Smalley, *J. Am. Chem, Soc.* **122**, 2383-2384 (2000).
50. L. Cai, J. L. Bahr, Y. Yao, J. M. Tour, *Chem. Mater.* **14**, 4235-4241 (2002).
51. D. Tasis, N. Tagmatarchis, A. Bianco, M. Prato, *Chem. Rev.* **106**, 1105-1107 (2006).
52. R. Barthos, D. Mehn, A. Demortier, N. Pierard, Y. Morciaux, G. Demortier, A. Fonseca, J. B. Nagy, *Carbon* **43**, 321-325 (2005).

53. G. S. Duesberg, R. Graupner, P. Downes, A. Minett, L. Ley, S. Roth, N. Nicoloso, *Synthetic Metals* **142**, 263-266 (2004).
54. S. B. Fagan, A. J. R. Silva, R. Mota, R. J. Baierle, A. Fazzio, *Physical Review* **B67**, 033405 (2003).
55. W. H. Lee, S. J. Kim, W. J. Lee, J. G. Lee, R. C. Haddon, P. J. Reucroft, *Applied Surface Science* **181**, 121-127 (2001).
56. H. Hu, B. Zhao, M. A. Hamon, K. Kamaras, M. E. Itkis, R. C. Haddon, *J. Am. Chem. Soc.* **125**, 14893-14900 (2003).
57. J. L. Bahr, J. M. Tour, *J. Mater. Chem.* **12**, 1952-1958 (2002).
58. M. Alvaro, C. Aprile, P. Atienzar, H. Garcia, *J. Phys. Chem.* **B109**, 7692-7697 (2005).
59. S. Niyogi, M. A. Hamon, H. Hu, B. Zhao, P. Bhowmik, R. Sen, M. E. Itkis, R. C. Haddon, *Acc. Chem. Res.* **35**, 1105-1113 (2002).
60. B. Parekh, G. Fanchini, G. Eda, M. Chhowalla, *Applied Physics Letters* **90**, 121913/1-121913/3 (2007).
61. J. E. Riggs, Z. Guo, D. L. Carroll, Y. P. Sun, *J. Am. Chem. Soc.* **122**, 5879-5880 (2000).
62. J. Chen, M. A. Hamon, H. Hu, Y. Chen, A. M. Rao, P. C. Eklund, R. C. Haddon, *Science* **282**, 95-98 (1998).
63. R. Czerw, Z. Guo, P. M. Ajayan, Y. P. Sun, D. L. Carroll, *Nano Letters* **1**, 423-427 (2001).
64. Z. Jin, X. Sun, G. Xu, S. H. Goh, W. Ji, *Chemical Physics Letters* **318**, 505-510 (2000).
65. M. Sano, A. Kamino, S. Shinkai, *Angew. Chem. Int. Ed.* **40**, 4661-4663 (2001).
66. Z. Konya, I. Vesselenyi, K. Niesz, A. Kukovecz, A. Demortier, A. Fonseca, J. Delhalle, Z. Mekhalif, J. B. Nagy, A. A. Koos, Z. Osvath, A. Kocsonya, L. P. Biro, I. Kiricsi, *Chemical Physics Letters* **360**, 429-435 (2002).
67. Y. Lin, A. M. Rao, B. Sadanadan, E. A. Kenik, Y. P. Sun, *J. Phys. Chem.* **B106**, 1294-1298 (2002).
68. I. Yamaguchi, T. Yamamoto, *Materials Letters* **58**, 598-603 (2004).
69. B. Parekh, T. Debies, C. M. Evans, B. J. Landi, R. P. Raffaelle, G. A. Takacs, *Mater. Res. Soc. Symp. Proc.* **887**, 3-8 (2006).
70. B. Parekh, T. Debies, P. Knight, K. S. V. Santhanam, G. A. Takacs, *J. Adhesion Sci. Technol.* **20**, 1833-1846 (2006).
71. M. Krysak, B. Parekh, T. Debies, R. A. DiLeo, B. J. Landi, R. P. Raffaelle, G. A. Takacs, *J. Adhesion Sci. Technol.* **21**, 999–1007 (2007).
72. J. D. Harris, R. P. Raffaelle, T. Gennett, B. J. Landi, A. P. Hepp, *Mater. Sci. Eng.* **B116**, 369–374 (2005).
73. R. A. DiLeo, B. J. Landi, R. P. Raffaelle, *J. Appl. Phys.* **101**, 064307/32–064307/36 (2007).
74. R. A. DiLeo, RIT Undergraduate Research Symposium, August (2005).
75. J. G. Calvert, J. N. Pitts, *Photochemistry.* John Wiley & Sons, New York, NY (1966).
76. B. J. Finlayson-Pitts, J. N. Pitts, *Chemistry of the Upper and Lower Atmosphere*. Academic Press, New York, NY (2000).

77. L. Oliveira, T. Debies, G. A. Takacs, in: *Nanotubes, Nanowires, Nanobelts and Nanocoils - Promise, Expectations and Status*, P. Bandaru, S. Grego, I. Kinloch (Eds.) *Mater. Res. Soc. Symp. Proc.* **1142**, in press, Warrendale, PA (2009).
78. G. A. Takacs, G. P. Glass, *J. Phys. Chem.* **77**, 1182 (1973).
79. H. Okabe, *Photochemistry of Small Molecules*. John Wiley & Sons, New York, NY (1978).
80. http://www.chem.qmul.ac.uk/surfaces/scc/scat5_3.htm
81. J. R. McNesby, H. Okabe, in: *Advances in Photochemistry*. Interscience Publishers, New York, NY (1964).
82. B. J. Finlayson-Pitts, J. N. Pitts, *Atmospheric Chemistry*. Wiley & Sons, New York, NY (1986).
83. N. A. Asrian, G. N. Bondarenko, G. I. Yemelianova, L. Y. Gorlenko, O. I. Adrov, R. Marassi, V. A. Nalimova, D. E. Sklovsky, *Mol. Crystl. Liquid Crystl. Sci. Technol., Section A:* **340**, 331-336 (2000).
84. J-L. Li, K. N. Kudin, M. J. McAllister, R. K. Prud'homme, I. A. Aksay, R. Car, *Phys. Rev. Lett.* **96**, 176101 (2006).
85. N. Yao, V. Lordi, S. X. C. Ma, E. Dujardin, A. Krishnan, M. M. J. Treacy, T. W. Ebbesen, *J. Mater. Res.* **13**, 2432-2437 (1998).
86. W. Zhou, Y. H. Ooi, R. Russo, P. Papanek, D. E. Luzzi, J. E. Fischer, M. J. Bronikowski, P. A. Willis, R. E. Smalley, *Chem. Phys. Lett.* **350**, 6-14 (2001).
87. A. M. Rao, J. Chen, E. Richter, U. Schlecht, P. C. Eklund, R. C. Haddon, U. D. Venkateswaran, Y. K. Kwon, D. Tomanek, *Phys. Rev. Lett.* **86**, 3895-3898 (2001).
88. J. L. Bahr, J. M. Tour, *J. Mater. Chem.* **12**, 1952-1958 (2002).
89. G. Beamson, D. Briggs, *High Resolution XPS of Organic Polymers: The Scienta ESCA300 Database*, Wiley, Chichester (1992).
90. J. F. Moulder, W. F. Stickle, P. E. Sobol, K. D. Bomben, in: *Handbook of X-ray Photoelectron Spectroscopy*, J. Chastin, R. C. King Jr. (Eds), p. 216, Physical Electronics, Eden Prairie, MN (1995).
91. J. A. Samson, *Techniques of Vacuum Ultraviolet Spectroscopy*, John Wiley & Sons, New York (1967).
92. M. Heintze, V. Bruser, W. Brandl, G. Marginean, H. Bubert, S. Haiber, *Surf. Coat. Technol.* **174**, 831-834 (2003).
93. V. Bruser, M. Heintze, W. Brandl, G. Marginean, H. Bubert, *Diamond Related Mater.* **13**, 1177-1181 (2004).
94. A. F. Perez-Cadenas, F. J. Maldonado-Hodar, C. Moreno-Castilla, *Carbon* **41**, 473-478 (2003).